Multi-influential interactions alters behaviour and cognition through six main biological cascades in Down syndrome mouse models

Arnaud Duchon[1,2,3,4], Maria del Mar Muñiz Moreno[1,2,3,4], Sandra Martin Lorenzo[1,2,3,4], Márcia Priscilla Silva de Souza[1,2,3,4], Claire Chevalier[1,2,3,4], Valérie Nalesso[1,2,3,4], Hamid Meziane[5], Paulo Loureiro de Sousa[6], Vincent Noblet[6], Jean-Paul Armspach[6], Veronique Brault[1,2,3,4] and Yann Herault[1,2,3,4,5]

[1] Institut de Génétique et de Biologie Moléculaire et Cellulaire, department of translational medicine and neurogenetics 1 rue Laurent Fries, 67404 Illkirch Graffenstaden, France

[2] Centre National de la Recherche Scientifique, CNRS UMR 7104, Illkirch Graffenstaden, France

[3] Institut National de la Santé et de la Recherche Médicale, INSERM U964, Illkirch Graffenstaden, France

[4] Université de Strasbourg, Illkirch Graffenstaden, France

[5] Institut Clinique de la Souris (ICS), CELPHEDIA, PHENOMIN, 1 rue Laurent Fries, 67404 Illkirch Graffenstaden, France

[6] Université de Strasbourg, CNRS UMR 7357, ICube, FMTS, Strasbourg, France

*Corresponding author:

Email: herault@igbmc.fr

Keywords: Down syndrome, mouse model, partial trisomy 21, Down syndrome critical region, genotype–phenotype maps, learning, memory, transcriptomics.

Short title: Neuronal altered pathways in Down syndrome mouse models

Abstract

Down syndrome (DS) is the most common genetic form of intellectual disability caused by the presence of an additional copy of human chromosome 21 (Hsa21). To provide novel insights into genotype–phenotype correlations, we screened the *in vivo* DS mouse library with standardized behavioural tests, magnetic resonance imaging (MRI) and digged into hippocampal gene expression. Altogether this approach brings novel insights into the field. First, we unravelled genetic interactions between different regions of the chromosome 21 and how they importantly contribute in altering the outcome of the phenotypes. Then, in depth analysis of misregulated expressed genes involved in synaptic dysfunction highlitghed 6 biological cascades centered around DYRK1A, GSK3β, NPY, SNARE, RHOA and NPAS4. Finally, we provide a novel vision of the existing altered gene-gene crosstalk and molecular mechanisms targeting specific hubs in DS models that should become central to advance in our understanding of DS and therapies development.

Author Summary

Down syndrome (DS) is the most frequent cause of intellectual disability and is caused by increase in gene dosage and multiple genetic interaction but not so many have been described so far. Taking advantage of DS mouse models, we investigated behavior and cognition, brain morphology and hippocampal gene expression in a controlled environment and we unraveled how multiple genetic interactions between different regions of the chromosome 21 contribute in altering the outcome of the behavioural, morphological and molecular/pathways phenotypes. Nonetheless we found multiple deregulated genes in the hippocampus, where overlapping DS models show convergence in the biological cascades altered, observed via building protein-protein interaction and regulatory networks, and centered in 6 main hubs: DYRK1A, GSK3β, NPY, SNARE, RHOA and NPAS4. Although four of them were already described to be altered in some DS models, we validated two additional ones, RHOA and NPAS4, and we have built a novel vision of

the existing altered gene-gene crosstalk and molecular mechanisms, targeting 6 specific highly interconnected hubs in DS models, that should become central to advance in our understanding of DS physiopathology and therapy development.

Introduction

Down syndrome (DS) is the most common genetic form of intellectual disability and was first described as a disease by John Langdon Down in 1866. One century later, genetic studies demonstrated that DS is caused by trisomy of human chromosome 21 (Hsa21) (1). People with DS have a wide range of phenotypic and physiological features with some phenotypic variability but always present several disabling features like mental retardation or Alzheimer disease (2). The leading cause of DS is non-disjunction of chromosome 21 (3). However, in rare cases, people with partial Hsa21 duplications are observed with a smaller spectrum of DS features. Studying these rare conditions increased our understanding of the genotype–phenotype correlations in DS (4-10). In particular, this method led to the hypothesis of the existence of a DS critical region (DCR) in which a small set of Hsa21genes (10) could play a major role in DS phenotypes, including cognitive disabilities. The understanding of DS has been substantially improved over the years, with the progress of genome analysis technologies. Recently, two studies showed that not a single trisomic region can be responsible for all DS features but rather several susceptibility regions when presented in 3 copies can induce a large variety of features (5, 7). In addition, recent publications showed that several patients displayed complex rearrangement like contiguous or non-contiguous deletions or duplications, copy number variations of other regions or duplication of genes located in the short arm of Hsa21, that can potentially impact the phenotypic outcome of the Hsa21 duplication and add noise to the genetic dissection of human trisomy 21 clinical manifestations.

To circumvent the difficulties in studying DS in human, several efforts have been made to generate DS mouse models (11). Indeed, there are three independent mouse genomic regions

carrying altogether 158 protein-coding homologous genes of the 218 protein-coding genes located on the Hsa21, including two keratin clusters of respectively 37 and 13 genes (12). The largest region homologous to Hsa21 is found on the mouse chromosome 16 (Mus musculus 16, noted as Mmu16) in a fragment of 22.42 Mb with 119 orthologous genes between *Lipi* and *Zbtb21* (13). The most telomeric part is splitted into two parts. The first part, on the mouse chromosome 17 (noted as Mmu17) with 19 homologous genes in 1.1 Mb interval between *Umodl1* and *Hsf2bp*. Then, the second part, on the the mouse chromosome 10 (Mmu10) with 37 genes included in the 2.3 Mb *Cstb-Prmt2* genetic interval (11, 12, 14). Several DS mouse models have been generated over the years, most of them were carrying trisomy of the largest genetic region located on Mmu16, and have built the *in vivo* DS mouse library (11, 14). The Ts(17^{16})65Dn (noted Ts65Dn) is the most widely used DS model and it is quite unique with a supplementary mini-chromosome obtained by x-ray irradiation of the male germline and containing the centromeric region of Mmu17, with genes from *Psid-ps2* to *Pde10a*, and the 13.5 Mb telomeric fragment of Mmu16 containing genes between *Mrpl39* and *Zbtb21* (15-18). Several models were made by chromosomal engineering (11) and carry segmental duplication of Mmu16. The Dp(16*Lipi-Zbtb21*)1Yey (noted Dp1Yey) corresponds to the duplication of the entire Mmu16 region syntenic to Hsa21 (19). The Dp(16Cbr1- Fam3b)1Rhr (noted Dp1Rhr) model carries a duplication from *Cbr1* to *Fam3b* and demonstrate the contribution of the DS critical region (DCR) (20-23). All the DS mouse models displayed defects in behaviour and cognition which had been investigated in different laboratories with different protocols and environmental condition making difficult inter-model comparison (11).

In order to improve our knowledge on DS, we analysed a series of old and new combinations of mouse models with a unique and in depth behaviour, morphological and transcriptomics pipeline in adults to dissect the contribution of the genes located on Mmu16 to DS mouse features. The behaviour pipeline relied on assessing specific brain functions found altered in people with DS and in particular those depending on the hippocampus (24, 25),. Thus,

we performed hippocampal-based learning tests together with other standardized protocols including the Y-maze, Open field (OF), Novel Object Recognition (NOR), Morris Water Maze (MWM) and contextual and cue Fear Conditioning (FC). All procedures were carried in similar environmental conditions to reduce any impact (26, 27). Besides, variations in specific brain regions have been observed in people with DS and mouse models (28-31). Neuroanatomical changes affect the whole brain volume or specific regions like the frontal region of the limbic lobe or the hippocampus in people with DS. Thus, we performed an in depth morphological investigation of the brain by magnetic resonance imaging (MRI). Finally, whole gene expression was performed on hippocampi isolated from all the models to decipher the genes, functional pathways and biological cascades affected in the different DS mouse models. Moreover, we identified the gene expression and functional profiles conserved in post-mortem patients brain derived datasets publicly available in the GEO database.

Results

Dissecting the contribution of Mmu16 subregions to the DS-related behavioral phenotypes in mouse models

We wanted to dissect the contribution of sub-regions located in the telomeric part of *Mus musculus* chromosome 16 (Mmu16), homologous to human chromosome 21 (Hsa21); (32), to the DS-related cognitive phenotypes in the mouse. First, we selected 4 DS mouse models: the Ts65Dn, the most commonly used DS model (15), and three additional models that are carrying segmental duplications of well-defined sub-regions located on the Mmu16, the Dp1Yey (19), Dp3Yah (33) and Dp1Rhr (20). In addition, we engineered a new one, the Dp5Yah, corresponding to three functional copies of the genes included in the genetic interval between *Cyyr1* to *Clic6*. This model was crossed with the Dp1Rhr one in order to generate the Dp5Yah/Dp1Rhr (noted Dp5/Dp1) coumpound transheterozygote carrying a trisomic gene

content similar to the Ts65Dn for the genes located on the Mmu16. We also included a model carrying an additional copy of *Dyrk1a*, one of the driver genes for DS-related phenotypes (30, 34), and the Tg(*Dyrk1a*) combined with Dp5Yah model (noted Dp5-Tg) (Supplementary fig 1). We used standardized behavioral tests to study several aspects of learning and memory in mice including the Y-maze (working memory), the open field (exploration memory), the novel object recognition (recognition memory), the Morris water maze (spatial memory) and the fear conditioning (associative memory). For all the lines, independent cohorts of control and trisomic mouse littermates went through the pipeline at similar ages, then the resulting data were processed using standard statistical analyses (See supplementary material and methods for details). First, we assesed the potential existence of a background effect over the distribution of the measurements taken in the different tests. No difference between B6J or hybrid B6JC3B wild-type controls was observed over the Q-Q plots with the cumulative frequency. Then, we defined a unique wild-type reference range corresponding to 90% of all controls (see Supplementary Table 1, Supplementary fig 2).

Mice activity and working memory were evaluated in the Y-maze (Fig 1A). The number of arm entries in the Y-maze showed that only Tg(*Dyrk1a*) mutant line was hyperactive in this test while deficit in spontaneous alternation was found in Dp1Yey (35), Ts65Dn (36), Dp1Rhr and Tg(*Dyrk1a*) (37). The Dp5/Dp1 also showed a clear deficit in the percentage of spontaneous alternation as compared to littermate controls while Dp5Yah trisomic animals showed normal performance.

The patterns of exploratory activity and anxiety were assessed in the open field (Fig 1B). Ts65Dn, Tg(*Dyrk1a*) and Dp5-Tgpresented hyperactivity with an increased travelled distance compared to wild-type littermates, and support, for Tg(Dyrk1A), results obtained in the Ymaze. In addition, Ts65Dn mice displayed thigmotaxic behavior with incraesed distance travelled at the periphery.

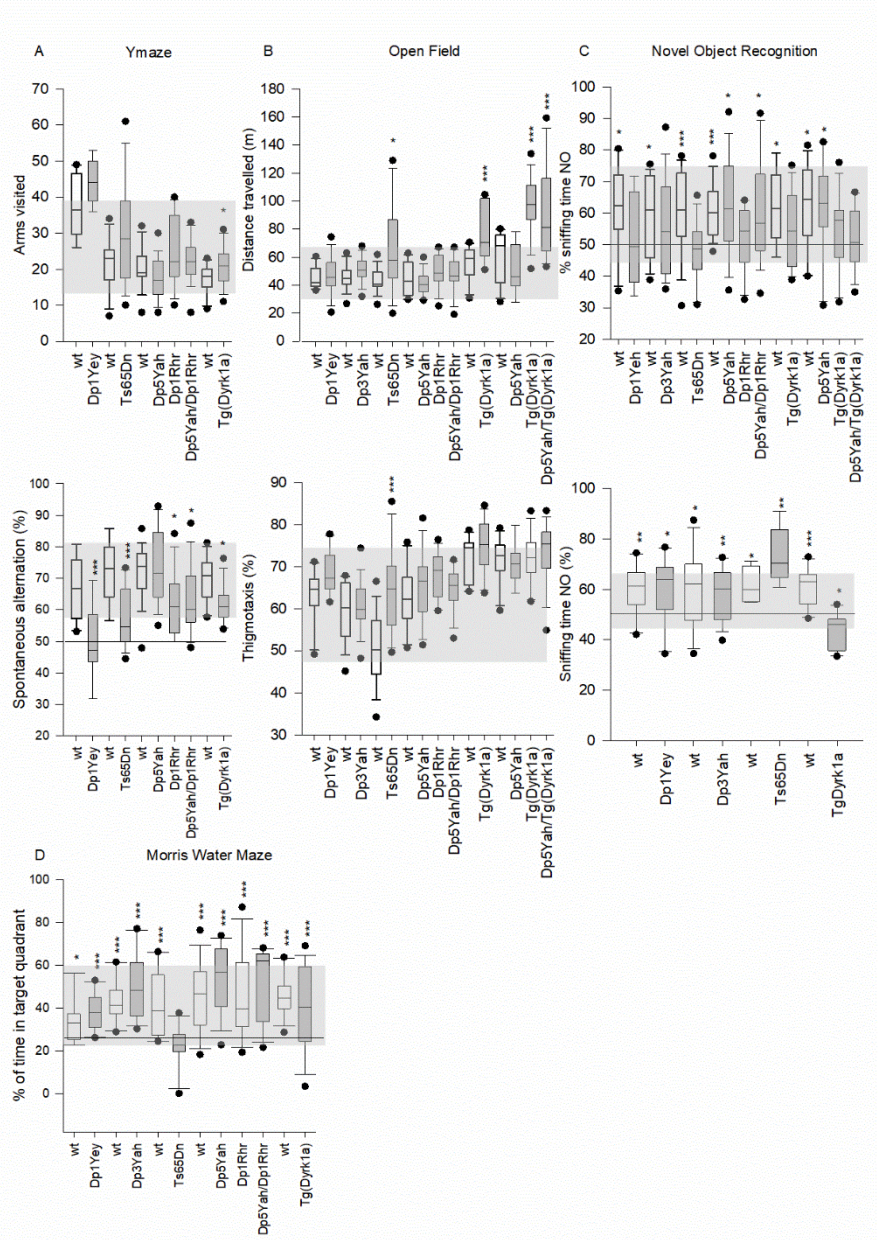

Figure 1. Standardized behavioural profiling of DS mouse models. Y-maze spontaneous alternation. Arm visited (A upper panel) and alternation rate (A lower panel) are presented as box plots with the median and quartiles (upper and lower 90% confidence interval are indicated by a grey box). Only the Tg(*Dyrk1a*) mice were showed hyperactivity in this test with increased arms entries compared to the wild type (p=0,017). Alternation rate in Dp1Yey (p=0,002), Ts65Dn (p<0,001), Dp1Rhr (P=0,012), Dp5/Dp1Rhr (p=0,018) and Tg(*Dyrk1a*) (P=0,010) mice was significantly lower than respective wild-type mice. Exploratory activity in a novel environment. Distance travelled (B upper panel) and % of distance travelled in peripheral zone recorded in the Open field arena (B lower panel). The total distance travelled was significantly higher in Ts65Dn (p=0,022), Tg(*Dyrk1a*) (p=0,008) and Dp5Yah/Tg(*Dyrk1a*) (p>0,001). Moreover, the % of distance in the peripheral zone was increased in Ts65Dn (p>0,001) mice comapred to wild type mice. Novel Object Recognition for 24 hour time lapse (C upper panel) and 1 hour time lapse (C lower panel). The results are presented as % of sniffing time (as box plots with the median and quartiles) for the novel object (NO). For 24 hours time laps, one sample t test vs 50% (hazard) showed that Dp1Yey (p=0,837), Dp3Yah (P=0,173), Ts65Dn (p=0;432), Dp1Rhr (p=0,492), Tg(*Dyrk1a*) (p=0,144) and Dp5Yah/Tg(*Dyrk1a*) (P=0,488) failed to recognize the new object. The Dp5Yah genomic fragment restored the capacity of the Dp1Rhr in the Dp5Yah/Dp1Rhr mice (p=0,0157). For 1 hour time laps, all the mice were able to discriminate the NO except for the Tg(*Dyrk1a*) (p=0,011 preference for FO). Probe test session in Morris Water Maze (D). The results are presented as % of time in the target quadrant. All the mice have spent more time in the target quadrant versus non target excepted for the Ts65Dn mice (p=0,398) (* p<0.05, **p<0.01, ***p<0.001).

The spatial reference memory was tested in the standard Morris water maze (MWM) task, in which mice have to escape from a circular pool of opaque water by localising a hidden platform at a single fixed location using distal spatial cues. We analysed the velocity, the distance travelled by the mice to reach the platform and the thigmotaxis over training (Supplementary fig 3). The velocity of Dp1Yey and Dp5Yah, was slightly lower than the wild-type mice (Supplementary fig 3B). As previously described (22, 38-44), Ts65Dn mice displayed a longer distance travelled to find the platform during all the sessions, compared to the wild type (Supplementary fig 3A). Although Tg(*Dyrk1a*) were able to locate the platform, they also showed delayed acquisition compared to the control mice. Surprisingly, the Dp1Yey, Dp1Rhr, Dp5Yah and Dp3Yah completed this test without any difference with the wild type group. Retention of place location was evaluated during a single probe trial (PT) with no platform available, 24h after the last training session (Fig 1D). The results confirmed as previously shown, that all the mouse strains except the Ts65Dn, remembered where the platform was located after the learning sessions. Interestingly, the Ts65Dn model, and to a lower extend the Tg(Dyrk1a) one, presented marked thigmotaxic behaviour, spending higher percentage of time in the peripheral zone as compared to controls (Supplementary fig 3C). Finally, to check the visual ability of mice, we performed a visual training version of the MWM during which the platform postion is indicated by a flag. All mice were able to find the visible plateform without any significant difference with controls except for the Tg(*Dyrk1a*) that presented a small delay in session 2 (Supplementary fig 3A).

We then evaluated non-spatial recognition memory using the novel object recognition (NOR) paradigm with the retention time of 24h. The percentage of sniffing time for the novel object was analysed and compared to 50% (hazard). This analysis showed that Dp1Yey, Dp3Yah, Ts65Dn, Dp1Rhr and Tg(*Dyrk1a*) were not able to discriminate the familiar and the novel objects unlike the Dp5Yah and more surpringly the Dp5/Dp1 (Fig 1C). to further

characterize the effect/lack of effect of Dp5Yah mutation on n ovel object recognition, the Dp5Yah mouse line was crossed with the Tg(*Dyrk1a*) and compared to new sets of wild-type, Dp5Yah and Tg(Dyrk1a) mice . Interestingly, we found that the Dp5Yah/Tg(*Dyrk1a*) and as expected the Tg(*Dyrk1a*) displayed altered novel object discrimination while the Dp5Yah spent more time exploring the novel object than the familiar one. We also assessed Dp1Yey, Dp3Yah, Ts65Dn and Tg(*Dyrk1a*) short term memory performing the NOR with 1 hour delay between acquisition and retention and only the Tg(*Dyrk1a*) mice showed a deficit.

All the trisomic lines were also tested for associative memory in the Pavlovian fear conditionning test. All the groups showed higher percentage of freezing during the 2 min post-shock compared to the habituation session, indicating that all groups developped fear responses during the training session (Supplementary fig 4). When animals were re-exposed 24 h later to the same context, the level of freezing in all groups was increased compared to the habituation (PRE2 and PRE4). However, freezing time for Ts65Dn mice was lower compared to the respective control littermates. When we assessed cued fear conditioning in a new context, all the mice presented an increased time of immobility with a strong difference between pre-cue and cue periods (Supplementary fig 4). In addition, Dp1Yey and slightly Ts65Dn showed lower freezing during presentation of the cues as compared to wildtype counterparts. These data suggest altered emotional associative memory Ts65Dn.

Dissecting the contribution of Mmu16 sub-regions to the DS-related brain morphological phenotypes in mouse models

DS models have been reported to show brain morphological alterations of specific regions (30). Thus, we wondered If we could detect changes in the brain morphology using MRI on these different partial trisomic mice models. Data were first analyzed using a volume approach and a brain region atlas. We confirmed that the brain of Tg(*Dyrk1a*) mice was larger ($p<0,001$) (30) and the brain of Dp1Yey mice was smaller than the respective wildtypes. Then,

we analyzed different brain regions/structures taking into consideration/correction the whole brain volume . Even with this correction, the Tg(*Dyrk1a*) mice were the most affected in terms of the brain structures volume, and on the contrary, the Dp1Rhr mice did not show any significant variation compared to the wt mice. Several regions, such as the basal forebrain septum, central gray matter, the rest of midbrain, and superior colliculi were significantly larger in Tg(*Dyrk1a*), Ts65Dn and Dp1Yey DS models. Moreover, the cerebellum, hypothalamus, inferior colliculi and caudate putamen were significantly different in Dp1Yey and Tg(*Dyrk1a*) compare to the control group (Supplementary Table 2, Supplementary fig 5) and a few additional areas were altered specifically in certain models (Amygdala, Globus pallidus, Hippocampus, Neo Cortex, and Thalamus for Tg(*Dyrk1a*); External capsule, Fimbria, and Ventricles for Dp1Yey). Altogether this brain morphometric analysis showed a greater similarity between Dp1Yey and *Dyrk1a* overexpression transgenic models with intermediate overlapp with the Ts65Dn mouse model.

Dissecting the contribution of Mmu16 subregions to the DS-related transcriptome phenotypes in mouse models

Various studies have shown the consequences of trisomy on gene expression (45-54). Here we took the opportunity to dissect the alteration of gene expression and functional pathways in various DS trisomic models carrying different duplications of the Mmu16. We analyzed the Ts65Dn, Dp1Yey, Dp3Yah, Dp5/Dp1, Dp5Yah, Dp1Rhr, and we included the trisomic model for *Dyrk1a* alone, Tg(*Dyrk1a*). Considering the hippocampal formation as a hub structure involved in learning and memory, we performed gene expression analysis in the adult hippocampus comparing the DS models with their own littermate controls using a unique pipeline for all the models. For each DS model, we defined the expressed genes (noted as EGs) as the genes whose expression level was detected, the differentially expressed genes (noted as

DEGs) as the genes whose expression level was found to be significantly altered in the trisomic model compared to the controls littermates, and then the trisomic expressed genes (TEGs) as the DEGs that are included inside the duplicated chromosomal regions for each model (Supplementary table 3, Table 1).

Mouse lines	Dp1yey	Dp3Yah	Ts65Dn (Mmu16)	Dp5/Dp1	Dp5Yah	Dp1Rhr	TgDyrk1A	Ts65Dn (Mmu17)
Nb of probes detected by the array					35556			
Nb of annotated probes detected (without control probes)					27359			
Number of trisomic genes detected by the array	155	21	130	127	87	40	1	40
Differential expressed genes (DEGs)	711	826	1074	922	736	1306	850	
Differential expressed trisomic genes (DETGs)	66	13	64	54	39	18	1	28
% of **DETGs	43%	62%	49%	43%	45%	45%	100%	70%
% of compensated trisomic genes detected	57%	38%	51%	57%	55%	55%	0%	
Number of GAGE KEGG and GOs (CC,BP,MF) terms disregulated in the trisomic model FDR<0.1	244	67	12	111	318	225	231	
Number of GAGE KEGG and GOs (CC,BP,MF) terms **upregulated** in the trisomic model FDR<0.1	207	60	3	33	4	132	222	
Number of GAGE KEGG and GOs (CC,BP,MF) terms **downregulated** in the trisomic model FDR<0.1	37	7	9	78	314	93	9	
Number of GAGE KEGG and GOs (CC,BP,MF) terms in the trisomic model unique to each mice line FDR<0.1	80	1	2	30	195	107	64	

*DEGs/DETs: Diferential expressed genes/ Diferential expressed
**DETGs/DETTs: Diferential expressed trisomic genes/

Table 1. Differential expression analysis results of the seven models analysed. DEGs are Differential Expressed Genes and TEGs for Differential Expressed trisomic genes. * Analysis done with Mmu17 and 16 trisomic genes. GO are Go functional terms involved in cellular compartment (CC), molecular function (MF) and biological processes (BP).

Although most of the genes in 3 copies were overexpressed in the relevant mouse model-derived hippocampi with a ratio around 1.5 (Supplementary fig 6), from 38% to 57% of the trisomic genes showed a dosage compensation (Table 1, Supplementary table 3). While this compensation is expected, we noticed that most of the compensated genes behave similarly in the different trisomic context, even if the experiments were done independently. As such the

genes from *Cldn17* to *Krtap11-1*, including the keratin cluster were not overexpressed when trisomic in any model (Dp1Yey, Ts65Dn, Dp5/Dp1 or Dp5Yah). This could be due to the fact that this region seems to be under strong regulatory constrains as on the borders two REST sites plus a LaminB1 peak encompassing this region were found (UCSC browser), while *Btg3* and *D16Ertd472e*, or *Mrpl39, Jam2, Atp5, Gabpa* and *App* are overexpressed in various DS models. We also found that the genes located on the trisomic segment not homologous to Hsa21 on the Mmu17 in Ts65Dn hippocampi, were overexpressed. (Supplementary fig 7) This fact is due to the trisomy of this region in the mouse line as previously reported in the mouse heart (16). Looking in detail into the homologous Hsa21 region in Mmu17, we saw two main genetic effects due to the overdosage of the Mmu16 region homologous to Hsa21. Noticeably, a constant deregulation of *Cbs* was found in all the models except Dp3Yah and Tg(*Dyrk1a*); suggesting a direct control of the *Cbs* transcription by at least two loci, one located in the Dp5Yah, and another one, not due to *Dyrk1a* overdosage, in the Dp1Rhr trisomic region. Similarly, under-expression of *Glp1r* was observed in Dp1Yey, Ts65Dn, Dp5/Dp1 and Dp5Yah while this gene was overexpressed in Dp1Rhr and not affected in Tg(*Dyrk1a*). Here too, *Dyrk1a* dosage was not involved, but at least two loci controlling *Glp1r* expression with opposite and epistatic effects should be found respectively in the Dp5Yah and Dp1Rhr genetic intervals.

The analysis of DEGs in each model separately highlighted the capabilities to separate the trisomic individuals from the wild-type littermates (Fig 2A) by principal component analysis (PCA), t-SNE (Fig 2B) or OPLS techniques (See supplementary material and methods).

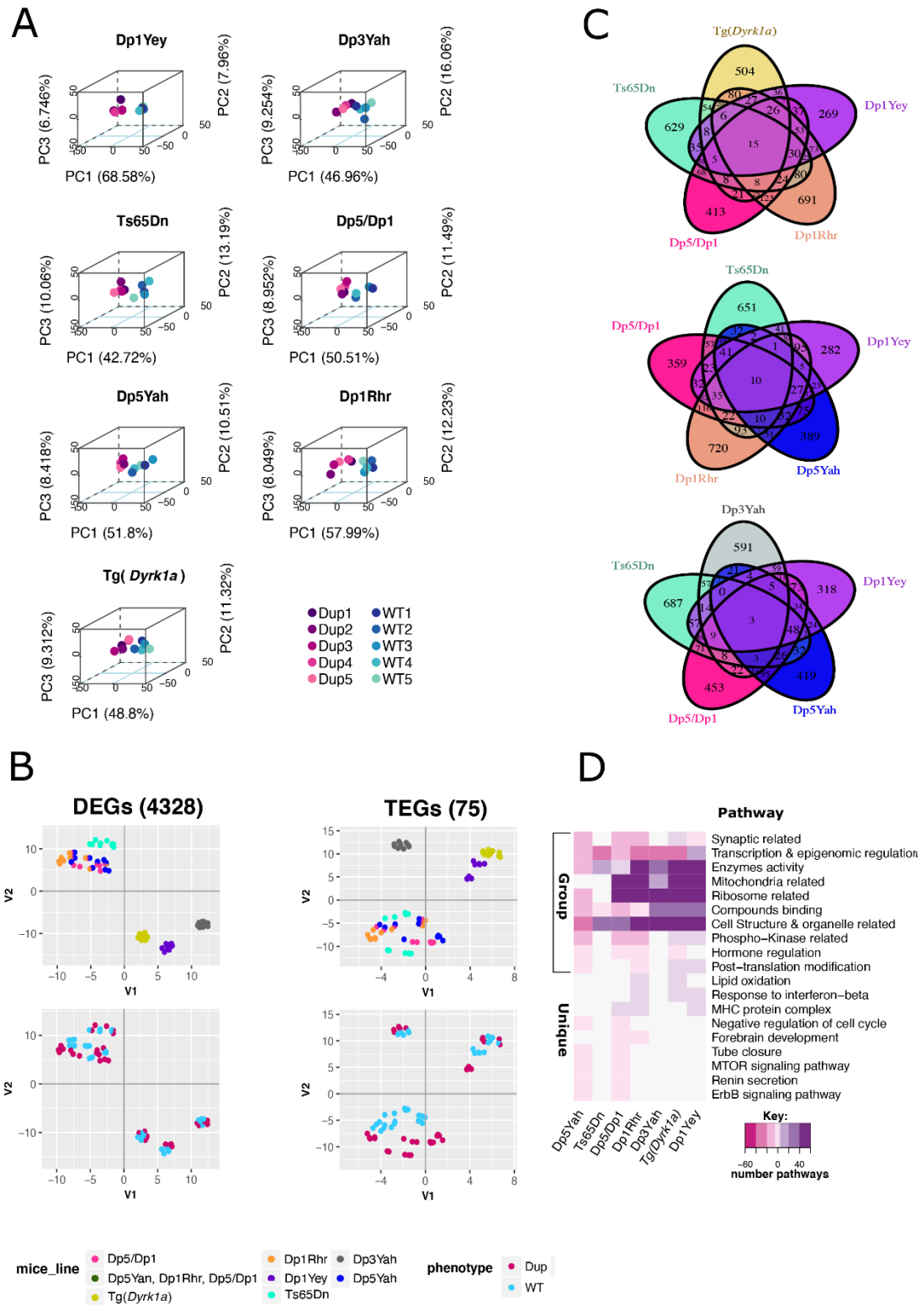

Figure 2: The differential expression analysis discriminates trisomic from disomic hippocampi and identifies common dysregulared genes and pathways. (A) 3D-PCA on the DEGs for each sample allows to separate trisomic (Dp) from disomic (wt) adult hippocampi. B) Left column: two dimensional Principal Component Analysis (2D-PCA) on the 5599 transcripts of the 4328 DEGs over all the samples identified using fcros 0.025<α<0.975. Right column: 2D-PCA on the 75 trisomic genes with a measured expression in all the models. (C) Venn Diagrams showing the overlap in gene expression between the different mouse lines represented in different colours. (D) Heatmap representation of the number and regulation sense

of the pathways shared at least by two mice lines identified using the genome expression for each mice line by GAGE R package and filtered by q-value cut off < 0.1. Grouped in the categories showed on the ordinate: synaptic related, synaptic related: representation of the pathways involved in Myelin sheath and SNARE complex formation, synaptic related: all the synaptic related pathways excluding myelin sheath and SNARE complex formation, Transcription & epigenomics regulation, Enzymes activity, Ribosome related, Mitochondria related, Cell Structure & organelle related, Phospho-kinase related… The color key breaks represents the number of pathways within the categories 60,40,20,5,0.5. The minus or pink color represents down regulated pathways, the white color represents no pathway found in the category and the purple or positive numbers stands for up regulated pathways respectively.

A genome-wide misregulation was found independently of the model, as DEGs were spread in all the chromosomes (Supplementary table 3-4, Supplementary fig 8), as shown previously (51), although with a stronger impact of the Dp1Rhr duplication on the number of total DEGs detected. The most overexpressed genes in terms of log2FC of expression and significance in various genetic conditions were visualised using Volcano plots (Supplementary fig 9, Supplementary table 4). For example, the *listerin E3 ubiquitin protein ligase 1* (*Ltn1*) gene, coding for a major component of the ribosome quality control and causing neurodegeneration in mice (55), was found overexpressed in Dp1Yey, Ts65dn, Dp5/Dp1, and Dp5Yah or *Ifnar2*, coding for the Interferon Alpha and Beta Receptor Subunit 2, is overexpressed as expected in models that carry three copies of this gene (Dp1Yey, Ts65Dn, Dp5/Dp1 and Dp5Yah). Instead, a more controlled gene like the *neuronal acetylcholine receptor subunit alpha-3* (*Chrna3*), is found upregulated only in Dp1Rhr and Dp1/Dp5, certainly due to the overexpression of one gene from the *Cbr1- Fam3b* region but not *Dyrk1a*. Nevertheless, when we performed the intersection between the list of DEGs from the different models, we only found a few genes in common (Fig 2C, Supplementary table 4). We decided to combine the analysis of all the lines together using PCA and t-SNE and revealed a strong clustering of models that share the same number of trisomic genes (Fig 2B). t-SNE analysis, based on 4328 DEGs, adding all DEGs detected in each mouse model together, showed different contribution of the various DS models to the transcriptome variation (Fig 2B, left panel) with 2 distinct groups: one encompassing four overlapping trisomies: Ts65Dn, Dp5/Dp1,

Dp5, Dp1Rh and three isolated models: Dp1Yey, Dp3Yah and Tg(*Dyrk1a*) that are closer together although Dp3Yah is clearly farthest from the other two. Similar distinct groups were seen when analysing the TEGs (Fig 2B, right panel) and overall, the trisomic and the wild-type individuals in each mouse line were nicely separated. As expected, the expression level of the TEGs and the DEGs in the different trisomic conditions were strongly correlated (Supplementary fig 10). Interestingly, the 4328 DEGs showed a level of mis-regulation strongly correlated between Dp1Yey and Dp3Yah (33%), Dp5/Dp1 (50%), Dp1Rhr (40%) and Tg(*Dyrk1a*) 42%. Of the 75 TEGS, the correlation was quite strong between Dp1Yey and Tg(*Dyrk1a*) with 28%. Thus, the correlation in gene deregulation showed that *Dyrk1a* overdosage is a key driver of transcriptome deregulation in the Dp1Yey and Dp1Rhr models. Unexpectedly, the correlation of DEGs mis-expression level was lower between Ts65Dn and Dp1Yey (29%) or Dp1/Dp5 (28%). On the opposite, a high number of TEGs are mis-regulated in the same way between Ts65Dn and Dp1Yey (49%) or Dp1/Dp5 (52%; Supplementary fig 10) suggesting that the other region found in 3 copies in the Ts65Dn over Mmu17 must be affecting the general DEGs landscape. We confirmed by qPCR the mRNA overexpression of first, *Dyrk1a* and *Sod1* genes in the DS models where they are trisomic; second, of *Synj2* and *Tiam2* that are located on the Mmu17 centromeric region in the Ts65Dn and third, of *Chrna1* a gene misregulated in Dp1Yey,Dp5/Dp1, Dp1Rhr and Ts65Dn models (Supplementary fig 15). As expected *Cbs*, expression was down regulated in all the models except Tg(*Dyrk1a*) and Dp3Yah. We also detected alterations of the expression of immediate early-response genes as *Arc*, *FosB*, *Fos* and *Npas4* that are important for cognition.

Differential functional analysis unravel a few common altered pathways in DS models

To go further, we performed a differential functional analysis and found 12 to 318 mis-regulated pathways in the DS models (table 1, Supplementary table 5). Interestingly, the sense of regulation of the overall deregulated pathways is trisomic region-dependent, as the Dp5Yah

(99%) region produced an overall downregulation whereas the Dp3Yah (89.5 %) and Dp1Rhr (56 %) regions together with the full Hsa21 syntenic model Dp1Yey (84.8 %), an upregulation. To facilitate the understanding, we clustered the broad functional dysregulation into 8 major functionality groups or meta-pathways. We found ribosomal components and mitochondrial processes pathways altered in all models with a high number of intermodel shared genes (Supplementary fig 12). Others meta-pathways like cell structure and organelles, transcription and epigenetic regulation, interferon and synaptic pathways were more affected in some models than in the others (Supplementary fig 13 and 14). As such, we observed strong and connected effects in the control of transcription and epigenetic regulation, enzyme activity and cell structure and cellular organelles involved in membrane and protein processing (endoplasmic reticulum, Golgi body, lysosome, peroxisome,…; Fig 2D) in the Dp1Yey, Dp5/Dp1, Dp1Rhr, and Tg(*Dyrk1a*) models, whereas the myelinization and 10 SNARE components, such as *Snap25* and *Snap23*, were specifically dis-regulated in the Dp1Yey Dp5Yah and Tg(*Dyrk1a*) models.

Interestingly, we saw a high number of shared genes between these pathways and the models giving rise to a high intermodel pathway connectivity. To assess the gene connectivity & cross talk, we build a protein-protein interaction (PPI) network of genes involved in synaptic function (noted MinPPINet) and furthermore we added regulatory PPIs to build the final RegPPINet. Then, we analysed the betweenness centrality to identify hubs, keys for maintaining the network communication flow that are most susceptible to targeted drugs attacks and the main signalling cascades affected. The relevance of the connecting nodes unknown to play a role in brain dysfunction, was further predicted by the machine learning algorithm Quack[118] and we found several evidences linking 449 (22 with a high confidence score) DEGs to GO/KEGG pathways involved in brain dysfunction, not previously known (Supplementary table 5). In fact, several evidences make us consider that those genes should be included in the

pathways:gene associations. Inside the evidences we can point that these DEGs were found dis-regulated in hippocampus, were included in the network built by STRING[73] as connecting nodes (not seeds) to produce a fully connected DS network, and their relevance to brain dysfunction was also predicted by Quack, in some cases, with a high score.

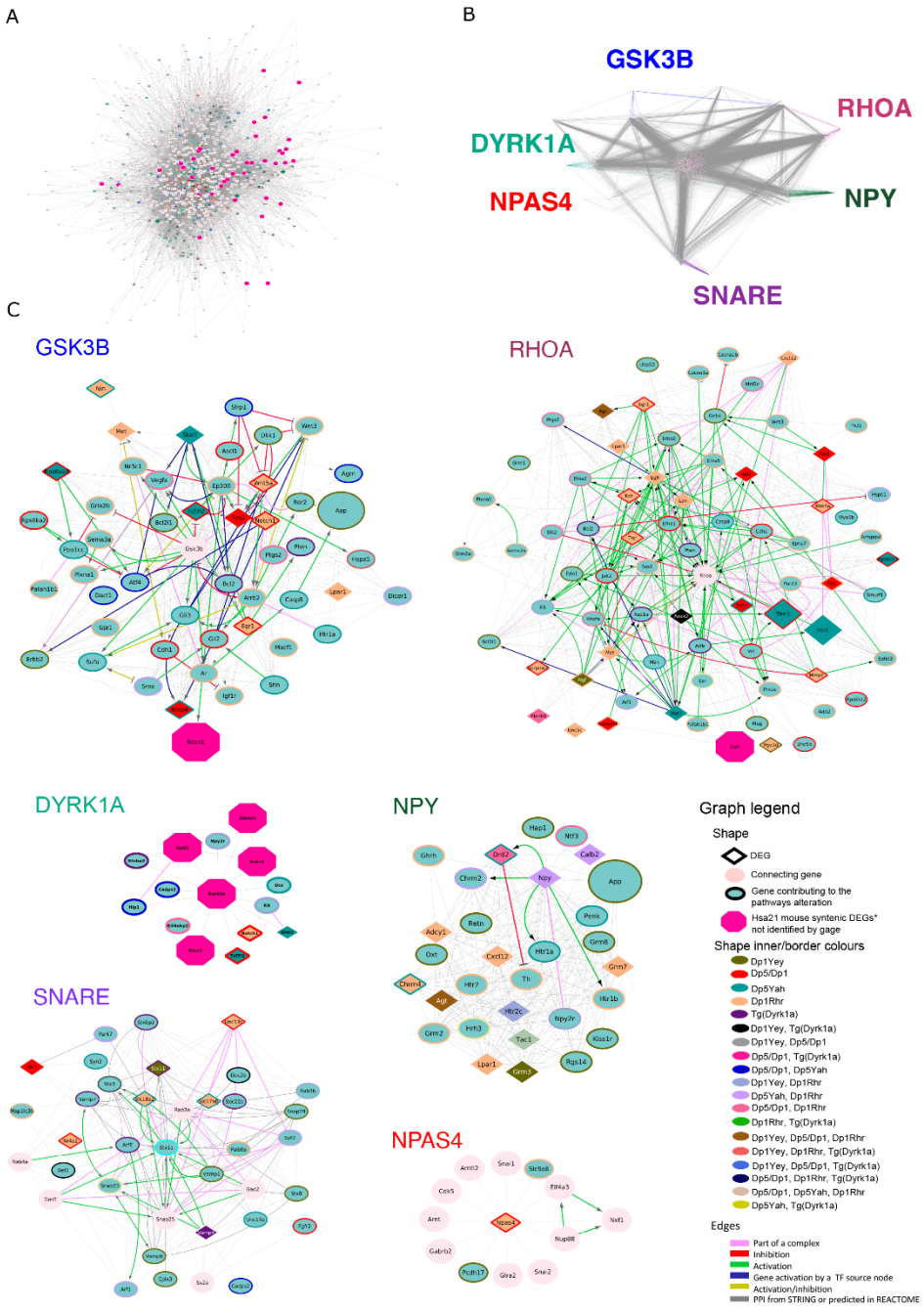

Figure 3: Protein-protein interaction networks involving DEGs linked to the synaptic function. (A) STRING04 MinPPINet of genes involved in synaptic function visualized using the edge weighed spring embedded layout by betwenness index in Cytoscape. The network was built by querying STRING and selecting the PPIs with a medium confidence score (CS=0.4) coming from all sources of evidence. The shapes of the nodes represent the following information: Shapes: i)Pallid pink ellipses: represent connecting proteins added to assure the

full connectivity of the network; ii) pink octagons, represent HSA21 syntenic genes in mouse not identified as contributing to the meta-pathway dysregulation by GAGE; iii) green inner coloured ellipses, genes identified by GAGE after q-val <0.1 cut off to be contributing even slightly, to any pathway of those found dysregulated inside the meta-pathway. If the size is similar to the octagons, they are also HSA21 syntenic genes in mouse. Additionally, the border colour represents the mouse model multi group where those genes are found altered in; iv) diamonds, genes identified by GAGE after q-val <0.1 cut off and also by FCROS as DEGs. (B) Network Structure Decomposition of the STRING04 MinPPINet. Highlighting in different colors the interactions of GSK3B, NPY, SNARE proteins, DYRK1A and RHOA respectively. In the case of NPAS4, the interactions coloured correspond up to the first level interactions. (C) The six RegPPINets were extracted from the selection of each fo the following proteins and their 2^{nd} interactors from STRING04 MinPPINet: RHOA, DYRK1A, GSK3B, NPY, SNARE proteins and NPAS4. Then, those were further annotated with regulatory information using REACTOME (See Supplementary material and Methods). The shapes of the nodes represent the following information: Shapes: i)Pallid pink ellipses: represent connecting proteins added to assure the full connectivity of the network; ii) pink octagons, represent HSA21 syntenic genes in mouse not identified as contributing to the meta-pathway dysregulation by GAGE; iii) green inner coloured ellipses, genes identified by GAGE after q-val <0.1 cut off to be contributing even slightly, to any pathway of those found dysregulated inside the meta-pathway. If the size is similar to the octagons, they are also HSA21 syntenic genes in mouse. Additionally, the border colour represents the mouse model multi group where those genes are found altered in; iv) diamonds, genes identified by GAGE after q-val <0.1 cut off and also by FCROS as DEGs. The edges colored represent the type of interaction annotated by following the PathPPI classification (Tang *et al.* 2015),and ReactomeFIViz annotations as follows i) The GErel edges indicating expression were colored in blue and repression in yellow. ii) PPrel edges indicating activation were coloured in green, inhibition in red. Iii) Interactions between proteins known to be part of complexes in violet. Iv) Predicted interactions were represented in grey including the PPI interactions identified by STRING DB (Szklarczyk *et al.* 2017) after merging both networks.

Looking into the DS synaptic MinPPINet (Fig 3A), first we analysed the DS network topography and betweenness connectivity and found hubs and genes more central for the network information flow. As expected from a PPI biological network, after computing 100000 random networks with a similar degree, the likelihood of observing such connectivity in the DS network was more than one can expect by chance (P-value < 2e-16) and it showed a small world effect and scale-free topology. Using a network decomposition approach (see supplementary material and methods), we highlighted 5 major subnetworks or biological cascades that strongly centralized 5 different proteins: DYRK1A, GSK3B, NPY, RHOA and SNARE proteins (Fig 3B-C). While DYRK1A is known to be central and was shown to have interaction with GSK3B and NPY in DS models (34, 56-60), the important role of SNARE complex proteins and the

biological cascade centred around RHOA for the pathophysiology of DS cognitive dysfunction is exposed by our analysis. Moreover, the network analysis showed that DYRK1A controls 42,3 % of the network nodes and 69,4 % of the network seeds, (DEGs known to be involved in brain synaptic pathways) via 2nd level interactors. Hence, DYRK1A could control the DS synaptic network via PPI and regulatory interactions. Furthermore, the biological cascades centred on GSK3B, DYRK1A and RHOA are highly interconnected (Supplementary fig 15) and in fact several interactors of RHOA are connected and could somehow modulate a higher percentage (75 and 68.5%) of the nodes of the network and synaptic seeds. Interestingly, *RhoA* was not found altered in the DEA analysis, instead was a node introduced in the network to have a fully connected synaptic PPI network. We checked whether the RHOA pathway was altered in the Dp1Yey and we found no changes in the expression of RHOA, confirming the transcriptomics analyses, but a significant decrease of the phosphorylation of the RHOA interactor Myosin light chain (P-MLC) in the Dp1Yey hippocampi compared to control. Thus, the RHOA pathways appeared to be down-regulated in the Dp1Yey DS mouse models (Fig 4A).

Npas4 pathway is up-regulated as a consequence of *Dyrk1a* overexpression

In our transcriptomics and network analysis, we found that *Npas4* was down-regulated in Tg(*Dyrk1a*), Dp1Rhr and Ts65Dn models and this gene level of expression is highly variable in the models (Supplementary fig 11). *Npas4* belongs to the class of immediate early genes with *Arc*, *Fosb* and *Fos*. Light deprivation and then exposure is known to drive robust gene expression, with shared early-response genes and distinct sets of late-response genes in excitatory and inhibitory (E/I) neurons (61). *Npas4* was recently identified as a key in E/I balance in the visual cortex after light deprivation (62).

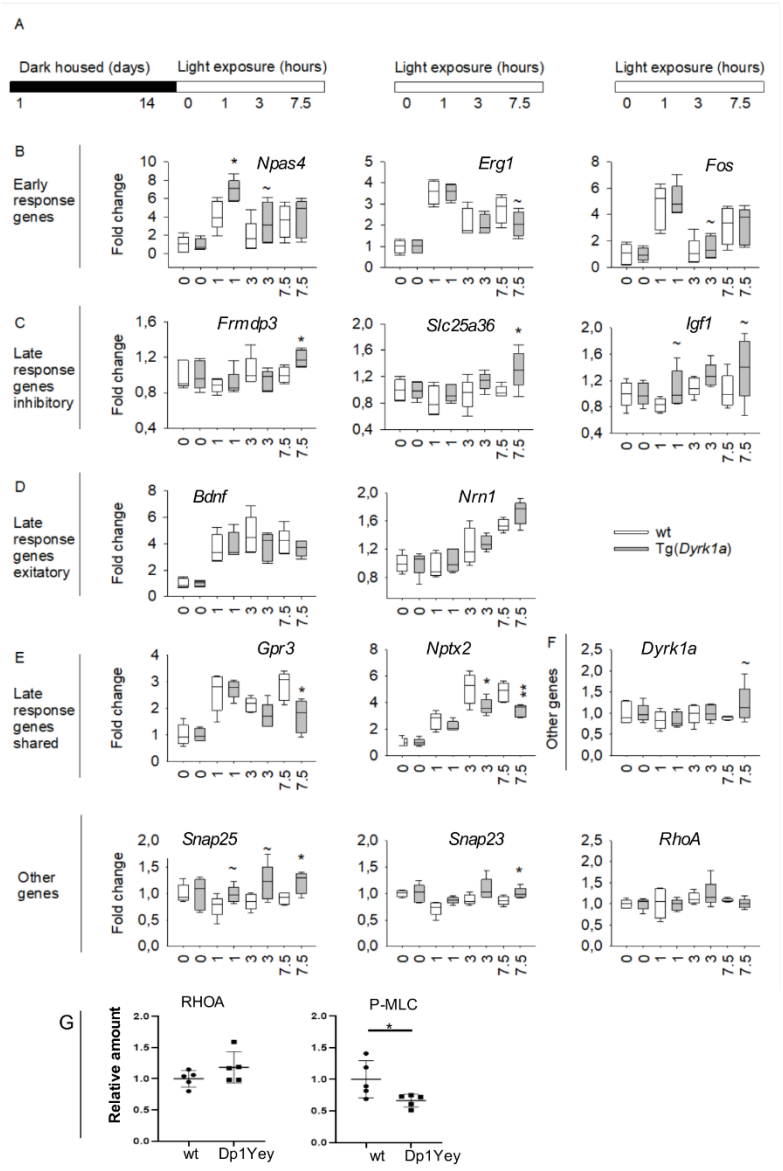

Figure 4: Evaluating Npas4 and RhoA pathways in DS models (A) RHOA pathway was altered in the Dp1Yey. Western blot analysis was revealed no changes in the expression of RHOA but a significant decrease of the phosphorylation of the Myosin light chain (P-MLC) in the Dp1Yey hippocampi compared to control. (B) Mice were housed in total darkness for 14 days and then were subsequently exposed to light for 0, 1, 3 or 7.5 h. Relative expression levels were determined, and fold change were calculated for each condition. Genotypes differences in fold change were assessed by T Test. (C) Only the fold change for early response genes *Npas4* was up-regulated in Tg(*Dyrk1a*) mice compared to wt at 1 hours of light induction. (D) The late responses genes specific to inhibitory neurons *Frmdp3*, *Slc25a36* and *Igf1* were up-regulated after 7.5 hours of light induction. (E) The fold change of late responses genes specific to excitatory neurons *Bdnf* and *Nrn1* were unchanged. (F) The fold change of late response genes shared by excitatory and inhibitory neurons *Gpr3* and *Nptx2* were downregulated after 3 and/or 7.5 hours of light induction. (G) *Dyrk1a* and *RhoA* showed a similar fold change along the different condition whereas *Snap25* and *Snap23* presented an increased enrichment for the 7.5 hours condition. Data are presented as box plots with the median and quartiles.

To confirm the impact of *Npas4* down regulation in Tg(*Dyrk1a*) mice, we performed qRT-PCR experiments to determine the specific early and late response genes altered in the visual cortex after light deprivation at 3 time points (1, 3 and 7.5 hours) after de novo light exposure (Fig 4B). The results showed that *Npas4* was clearly induced after light deprivation following 1 hour of light stimulation. Expression data revealed also a strong overexpression of *Npas4* following 1 hour of light stimulation in Tg(*Dyrk1a*) mice (Fig 4C). On the contrary, the

539 expression of late response genes specific for inhibitory neurons (*Frmdp3*, *Slc25a36* and *Igf1*,
540 Fig 4D) and late response genes (*Grp3* and *Nptx2*, Fig 4F*)* were altered after 7.5 hours of light
541 stimulation in Tg(*Dyrk1a*). Interestingly, late response genes specific to exitatory neurons (*Bdnf*
542 and *Nrn1*, Fig 4E) were not affected. The *Snap25*, *Snap23* candidate genes found in our analysis
543 showed an altered expression after 7.5hours of light stimulation while *Dyrk1a* and *RhoA* levels
544 were not affected (Fig 4G). These results indicate that inhibitory pathways controlled by *Npas4*
545 were affected by *Dyrk1a* overexpression. Furthermore, the network analyses highlighted
546 NPAS4 as a potential modulator of the synaptic dysfunction as via well connected interactors,
547 NPAS4 could affect the main altered biological cascades plus the GABA and NMDA receptors
548 involved in the modulation of the excitatory / inhibitory balance of the brain (61).
549

550 ## Discussion

551 In this study, we explored the in vivo DS mouse model library focusing on the region
552 homologous to Hsa21 found on Mmu16, to decode the DS genotype-phenotype relationships
553 and further underlie genetic interactions between different regions. For this, we assessed 6
554 partial DS trisomic models and a transgenic model overexpressing one copy of *Dyrk1a* using
555 a standardized behavioural pipeline focused on hippocampus-dependent memory processes. As
556 expected, we found deficits in the Ts65Dn mice similar to the ones previously published in the
557 Y-maze, the open field, NOR, MWM and contextual fear conditioning (36, 63) tests.
558 Strinkingly, thigmotaxis and time in the target quadrant in the probe test of the MWM were two
559 variables only modified in the Ts65Dn trisomic model while the Dp1Yey, that carry a
560 duplication of the complete syntenic Mmu16 region, was less affected as described before (64,
561 65). Interestingly, the Dp5Yah mice, duplicated for a chromosomic region from *Cyyr1* to *Clic6*,
562 present no deficits in all the tests done and have the lower number of DEGs. This might indicate
563 that the *Cyrr1-Clic6* region was not sufficient to induce by itself cognitive defects. However,
564 this syntenic region includes the genes *Sod1*, *Olig1*, *Olig2*, *Rcan1* and *Synj1*, proposed before

565 as inducing early DS cognitive phenotype (66-69). Curiously, no defects were found in the
566 Dp5/Dp1 mice contrary to the Ts65Dn in the open field or less severe in the NOR test. This
567 indicates the existence of a key modulator in the *Cyyr1-Clic6* region. The major behavioural
568 alterations found in the Ts65Dn could result from the influence of different factors. First, the
569 presence of the freely segregating mini-chromosome (70). Similarly, transcriptomic analysis
570 showed a different global disruption of the genome expression, compared to the other trisomic
571 models with segmental duplications. Then, the trisomy of about 60 Mmu17 centromeric genes
572 non homologous to Hsa21(16), overexpressed in the hippocampus of Ts65Dn mice,
573 highlighting specially *Tiam2* and *Synj2* that may exacerbate the effect of the overexpression of
574 *genes* located on the Mmu17 segment homologous to Hsa21 as *Tiam 1* and *Synj1*. *In fact,*
575 previous studies underline the strong role of *Synj1* in cognitive deficits of Ts65Dn (69, 71).
576 Moreover, the major differences in behavioral alterations could be the result of the syntenic
577 genes overexpressed in this model that have complex interactions with others. This is
578 emphasized by the low correlation of DEGs and deregulated pathways between Ts65Dn,
579 Dp1Yey and Dp5/Dp1. Finally, the presence of modulator genes, in the Dp5 region for example,
580 could alter the behavioral performance and gene expression landscape. In example, as suggested
581 by our genotype-phenotype analysis it seems to be a suppression of the effect of the *Mrpl39-*
582 *Zfp295* trisomy in the Dp1Yey model. In addition, several genes are deregulated only in Dp1Rhr
583 and Ts65Dn, and not in Dp5/Dp1, or vice versa, which can explain the rescue of episodic
584 memory in Dp5/Dp1 and highlights even more the complexity in gene interactions established
585 between the different trisomic regions.

586 In this unique comparison, we found that the spontaneus alternation in Y-maze, was
587 altered in all the models (except the Dp5Yah alone; Fig 5).

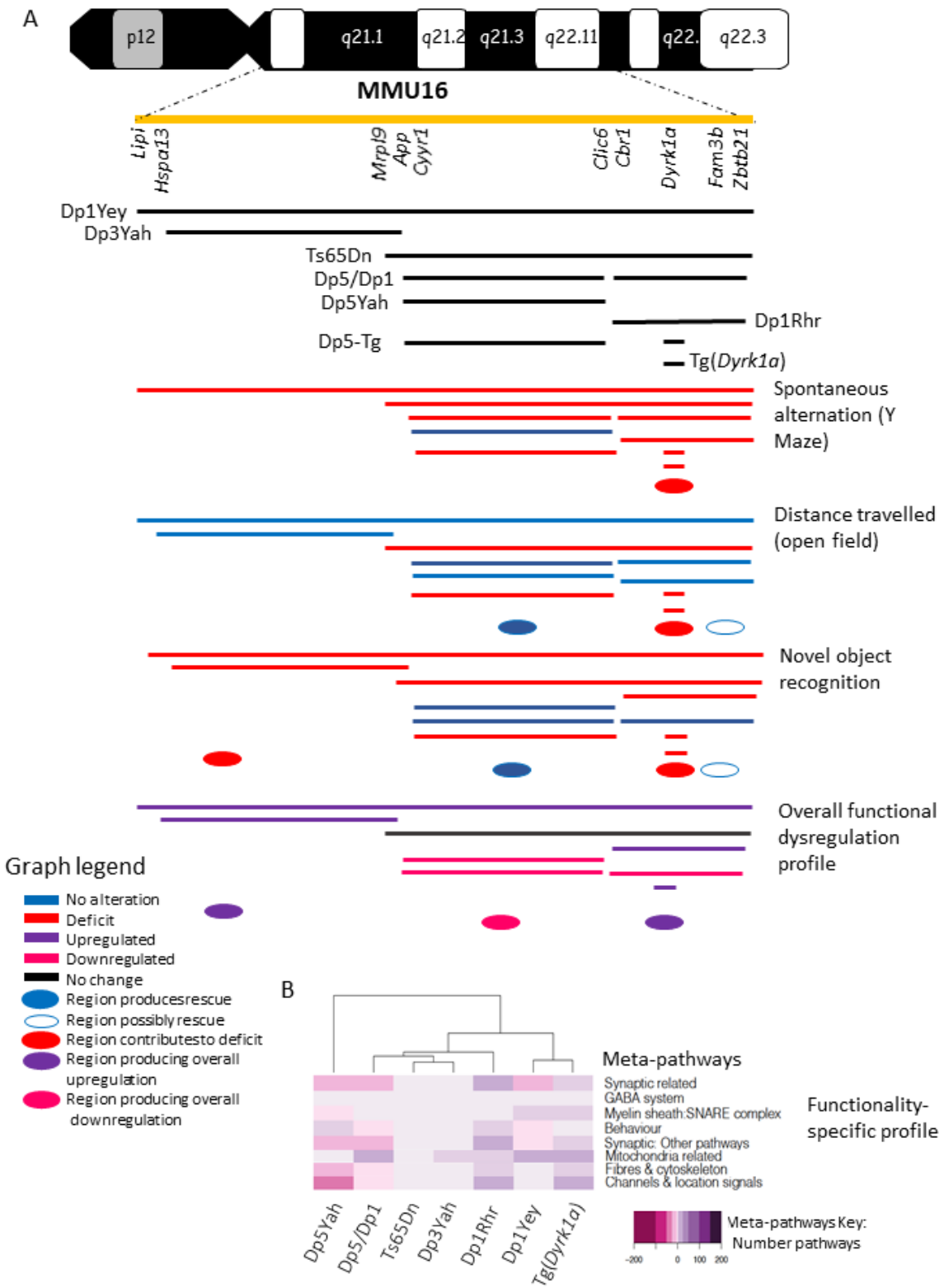

Figure 5: Genotype correlation associated to behaviour phenotype in partial trisomic DS model. Here we highlight the duplicated region carried on each model with the corresponding syntenic region in the human chromosome 21 together with the main behavioral and transcriptomics results pointing to the existence of region specific phenotypes and functional alteractions. The black lines represents the duplicated syntenic regions to human chromosome 21 on each model (represented in the yellow line). The blue lines represents the behavioral

595 results where no alteration was found, instead the red lines identifed the tests with deficits. Over
596 the transcriptomics meta-pathways fucntional profile summary picture, in purple is highlighted
597 upregulation whereas in pink downregulation. The intensity of the color stands for the number
598 of pathways included on each meta-pathway from the total number of pathways found altered
599 on each model.
600

601 The minimal common genetic part of these lines was the overexpression of *Dyrk1a* and
602 the result observed for the transgenic Tg(*Dyrk1a*), altogether with results previously obtained
603 (72-74), support DYRK1A as a main driver of this DS cognitive phenotype (34). Similarly,
604 DYRK1A overdosage caused the increased exploration measured by the distance travelled in
605 the open field that was only affected in Ts65Dn, Dp5/Tg(*Dyrk1a*) and Tg(*Dyrk1a*).
606 Interestingly, the Dp1Rhr Ds model was not affected suggesting that another loci intefere with
607 *Dyrk1a* overdosage in this model and the situation should be even more complex as no
608 phenotype is observed for the distance travelled in the Dp5/Dp1 while the Ts65Dn showed an
609 increase in this variable. The novel object recognition with 24h of retention unravelled
610 deficiency in most of the models, except in the Dp5Yah and Dp5/Dp1, suggesting that there are
611 at least two causative loci: one located in the Dp3Yah region and *Dyrk1a*; and presumably two
612 modifier interacting loci: one located in the Dp5Yah and another in the Dp1Rhr regions (Fig
613 5). Altogether, the altered behavior and cognition observed in DS models results from the
614 interaction of several loci, spread along the Mmu16, including *Dyrk1a*. Moreover, as
615 summarized in Fig 5, our study highlights the existence of different degrees of genetic
616 interaction complexity for behavioural and brain morphology phenotypes.

617 Surpringly, brain morphology was less affected in Dp1Rhr compared to the other DS
618 models, while Dp1Yey, Ts65Dn and Tg(*Dyrk1a*) shared alterations in identical structures.
619 Changes were found in several regions including the basal forebrain septum, a predominant
620 source of cortical cholinergic input with an early substantial loss of basal forebrain cholinergic
621 neurons (BFCN) as a constant feature of Alzheimer's disease and other deficits in spatial
622 learning and memory (75). Individuals with DS exhibit progressive degeneration of BFCN (76).

Similarly, significant loss of BFCN is present in the Ts65Dn (for review see (77)) and moreover, our results seem to indicate a default in BFCN in Dp1Yey and Tg(*Dyrk1a*) too. Several findings suggest that overexpression of amyloid protein precursor (APP) play a major role and could be strictly necessary for BFCN cell loss (78), thus, future investigation in Tg(*Dyrk1a*) should reveal if BFCN loss is present even without APP overexpression. Besides, only the Ts65Dn present an enlargement on the ventricles, which was previously associated with a decrease of cortical neurogenesis in the brains of Ts1Cje and Ts2Cje mouse models (28).

Our comparative genome wide expression profiling in the mouse hippocampus revealed that not a single gene or a single region can recapitulate the whole disregulation. The overall effect results from a complex interplay of a few trisomic overexpressed genes and other genes spread along the genome, shown by the majority of DEGs not being Hsa21 genes (Supplementary table 3). Additionally, we identified 34 trisomic DEGs (TEGs) with regulatory activity (Transcription factors, chromatin modellers...) as *Mir99a, Usp16, Erg* or *Rcan1* that may be involved in the models' changed regulatory landscape. Indeed, *RCAN1* and *USP16* were found upregulated in all human brain datasets (cerebrum and cerebellum) and USP16 was also found as DEG upregulated in heart and adult fibroblasts while MIR99A was found upregulated in adult fibroblast (46). Nevertheless, the DEGs expression was strongly correlated and conserved in Mmu16 based DS models. This is similar to the behavioural results obtained where related phenotypes were found in models carrying correlated partial duplications. Unexpectedly, Dp1Yey DEGs correlation is closer to Tg(*Dyrk1a*) than to Ts65Dn (42% against 25%) and there is a negative correlation between Dp3Yah & Dp5Yah (22%) and Tg(*Dyrk1a*) & Dp5Yah (13%) pointing out to a different gene dysregulation and phenotype development on these models and to the existence of epistasis with some regulatory trisomic genes countering the effect of genes in other trisomic regions. Carrying an in depth functional annotation analysis, we could not find a unique common pathway altered in all models. Nevertheless, due to the high redundancy in both GO and KEGG terms and the genes associated with each term,

649 grouping the pathways shared at least by two models (materials & methods) in 8 functional
650 groups unravelled 8 major meta-pathways with ribosome and mitochondrial function,
651 transcription & epigenomics regulation, and the synapse function categories highly affected.
652 We also found a strong upregulation of genes involved in the InterferonB pathway
653 (Supplementary fig 13B) as some interferon receptors are found upregulated in Mmu16 DS
654 models. As such *Ifnar2* and *Il10rb* were found upregulated in all the mice lines (except
655 Tg(*Dyrk1a*)) pointing to a potentially critical role in the interferon pathway dysregulation. The
656 same was observed with other genes as *Irgn1,Ifit1, Ifit2* or *Ndufa13*. This upregulation of the
657 interferonB pathways was previously reported in the Ts1Cje mouse model (79, 80) and linked
658 to a possible increase of activity of the Jak-Stat signaling pathway as recorded here by the up
659 regulation of *Stat1*.

660 Expression of genes involved in long-term synaptic potentiation (LTP) and synaptic
661 plasticity were decreased in Dp1Yey, Dp5Yah, Dp1Rhr, Dp5/Dp1 models respectively,
662 corroborating previous reports in different DS mouse models and in vitro studies. The only
663 upregulated pathways were the myelin sheath and SNARE; both found in Dp1Yey and
664 Tg(Dyrk1A) models. Ten genes from the SNARE complex were dysregulated, from those, we
665 validated the disregulated expression of *Snap25* and *Snap23* by qRT-PCR. Interestingly,
666 models carrying the Dp1Rhr region duplication showed a dysregulation mainly in synapse
667 transmission, plasticity and LTP, while models carrying the Dp5Yah region duplication showed
668 a dysregulation associated with genes involved in stemness and differentiation. Together, the
669 models with both Dp5Yah & Dp1Rhr duplicated regions, were involved in post-synapse
670 modulation and transmission. Moreover, there is a high number of shared DEGs between these
671 pathways and the models giving rise to a high intermodel inter-pathway connectivity with genes
672 strongly connected into major subnetwork biological cascades centralized over 6 different
673 proteins DYRK1A, GSK3B, RHOA, NPY, NPAS4 and SNARE complex. These new cascades
674 may also play a crucial role in the brain dysfunction associated with the DS phenotypes.

675 Organizing the network to follow the betweenness centrality index values, RHOA, DYRK1A,
676 GSK3B, and their interactors were more closely knitted together and populated the central part
677 of the network while SNARE, NPAS4 and NPY with their first- and second-layer interactors
678 were more in the periphery of the network. This strong interconnectivity has a double
679 interesting effect, first it makes the full network really sensible to targeted attack against these
680 proteins and at the same time the network would be robust against the attacks if the attack does
681 not target several proteins simultaneously; for example during a drug trial. Thus, studying
682 further closely connected altered genes and understanding the interactions could provide novel
683 insights into the possible molecular mechanism explaining why so many compounds, including
684 DYRK1A specific kinase inhibitors, can restore learning and memory in DS models (35, 81-
685 83). Additionally, these nodes show a high number of connections. Indeed, organising the
686 network using the betweenness index, these nodes and their interactors occupy the centre of the
687 network showing the extreme importance of these nodes for the stability of the network in terms
688 of network theory. Moreover, similar to the observation in DS patients, where the
689 affectation/severity of the gene dysfunction vary for one patient with partial duplications to the
690 other, we proposed here that different DS mouse models show different signalling cascades that
691 were affected with several members strongly interconnected and affecting brain dysfunction
692 leading to similar behavioural phenotypes; may be one possible explanation of the
693 developmental instability hypothesis, which postulates that the non specific triplication of a
694 relative small number of genes causes genetic imbalance with wide impact on global gene
695 expression. This hypothesis should be taken into account when therapeutic assay are planned.
696 The result in one partial trisomic mouse model should be replicated in more genetically complex
697 models to test potential genetic influencial factor (35, 84, 85). This is probably the limit of the
698 model, even if the mechanisms of behaviour and memory are common between mice and
699 human, the complexity of the system is lower. Conducting the same studies in more complex

700 animal models, carrying all the trisomic genes homologous to Has21, probably would
701 definetely permit a better deciphering of genes impacting on cognitive behaviour.
702

703 # Material and Methods

704 ## Mouse lines

705 The duplications of different Mmu 16 regions (Dp(16*Lipi-Zbtb21*)1Yey (or Dp1Yey),
706 the Dp(16*Hspa13-App*)3Yah (noted Dp3Yah), the Dp(16*Cbr1- Fam3b*)1Rhr (or Dp1Rhr)) and
707 the BAC transgenic for *Dyrk1a* (Tg(*Dyrk1a*)) models were previously described (19, 20, 33,
708 86). The genetic background of the DS lines carrying each duplication was pushed toward the
709 C57BL/6J (B6J) genetic background for more than 7 generation of backcross. The only
710 exception is the trisomic Ts65Dn (Ts(17^{16})65Dn) mice, initially obtained from the Jax, that was
711 kept on a F1 B6C3B genetic background (with the C3B line as a C_3H/HeH congenic line for
712 the BALB/c allele at the *Pde6b* locus (87)). The Dp(16*Cyyr1-Clic6*)5Yah (noted Dp5Yah) was
713 generated by the *in vivo* TAMERE technology inserting loxP sites in *App* and *Runx1* (see
714 Supplementary information). In the Dp3Yah and Dp5Yah models, only 2 complete copies of
715 *App* and *Runx1* genes are expressed. The Dp5Yah line was crossed with the Dp1Rhr in order
716 to generate the Dp5Yah/Dp1Rhr (also noted Dp5/Dp1) coumpound transheterozygote carrying
717 a similar trisomic Mmu16 gene content to that of the Ts65Dn. Indeed, only 15 Hsa21
718 homologous genes (*Mrpl39, Jam2, Atp5j, Gabpa, App, Cyyr1, Runx1, Setd4, Mx2, Tmprss2,*
719 *Ripk4, Prdm15, C2cd2 and Zbpb21*) over 174 are not in 3 copies in Dp5/Dp1 compared to
720 Ts65Dn while the genes located on the Mmu17 telomeric regions trisomic in the Ts65Dn
721 minichromosome (16) are not trisomic in the Dp5/Dp1. The Dp5Yah model was also combined
722 with the Tg(*Dyrk1a*) by crossing Dp5Yah/+ and Tg(*Dyrk1a*)/0 animals and generating the four
723 genotypes (Dp1Yah, Dp5Yah, Tg(*Dyrk1*a) and [Dp5Yah; Tg(*Dyrk1a*)] noted here Dp5-Tg), to
724 test specific interaction between Dp5Yah and *Dyrk1a* overdosage.

All the lines were maintained under specific pathogen-free (SPF) conditions and were treated in compliance with the animal welfare policies of the French Ministry of Agriculture (law 87 848) and the phenotyping procedures were approved by our local ethical committee (Com'Eth, n°17, APAFIS n°2012-069).

Behaviour pipeline

A serie of behavioural experiments were conducted in mice with a range of age between 2,5 to 7 months, as described in the Supplementary information. The tests were administered in the following order: Y-maze, open field, novel object recognition (24h), Morris water maze and fear conditioning (contextual and cue). Behavioural experimenters were blinded to the genetic status of the animals. Separate groups of animals were composed for each line (as indicated in supplementary table 1). Several mouse models found defective for the NOR performed with 24h of retention memory were also tested after 1h of retention. The Dp5Yah crossed with Tg(*Dyrk1a*) was tested for Y-maze and NOR at 24h. All the standard operating procedures for behavioural phenotyping have been already described (85, 88-91) and are detailed in the supplementary information.

Magnetic Resonance Imaging

A dedicated cohort of animals at the age 102 +/- 7 days was anesthetized and perfused with 30 ml of room temperature 1X Phosphate Buffer Saline (PBS) complemented with 10% (% w/v) heparine and 2mM of ProHance Gadoteridol (Bracco Imaging, Courcouronnes, France) followed by 30ml of 4% PFA complemented with 2mM of ProHance Gadoteridol. Then the brain structure was dissected and kept in PFA 4% 2mM ProHance over night at 4°C. The next day, each specimen was transferred into 1X PBS 2mM ProHance until imaging.

Just prior to imaging, the brains were removed from the fixative and placed into plastic tubes (internal diameter 1 cm, volume 13 mL) filled with a proton-free susceptibility-matching

fluid (Fluorinert® FC-770, Sigma-Aldrich, St. Louis, MO). Images of excised brains were acquired on a 7T BioSpec animal MRI system (Bruker Biospin MRI GmbH, Ettlingen, Germany). Images were reconstructed using ParaVision 6.0. An actively decoupled quadrature-mode mouse brain surface coil was used for signal reception and a 72-mm birdcage coil was used for transmission, both supplied by Bruker. The first protocol consisted of a 3D T2-weighted rapid-acquisition with relaxation enhancement (RARE). The second imaging protocol consisted of a 3D T2*-weighted Fast Low Angle (FLASH) sequence. The image matrix for both sequences was 195 x 140 x 90 over a field of view 19.5 x 14.0 x 9.0 mm^3 yielding an isotropic resolution of 100 μm and was treated and analysed for anatomical parameters as detailed in the supplementary information.

Gene expression assay

Hippocampus were isolated from DS trisomic models and their littermate controls (N = 5 per group) and flash frozen in liquid nitrogen. Total RNA was prepared using the RNA extraction kit (Qiagen, Venlo, Netherlands) according to the manufacturer's instructions. The samples quality was checked using an Agilent 2100 Bioanalyzer (Agilent Technologies, Santa Clara, California, USA). Gene expression analysis was carried out using GeneChip® Mouse Gene 1.0 ST arrays (Affymetrix, Santa Clara, CA). All the procedure and the analysis are detailed in the supplementary information. Raw microarray data and re-analysed data have been deposited in GEO (Accession No. GSE149470).

Bioinformatic analysis

The gene expression profile of the mouse hippocampi isolated from Dp1Yey, Dp3Yah, Ts65Dn, Dp5/Dp1, Dp5Yah, Dp1Rhr and Tg(*Dyrk1a*) trisomic mouse models was analysed with a specific bioinformatic pipeline and controlled for quality prior and after the Data pre-processing and normalization (see supplementary information in the detailed material and

775 methods section). The identification of the differentially expressed genes (DEGs), was
776 performed using a method based on fold change rank ordering statistics (FCROS)(92). In the
777 FCROS method, k pairs of test/control samples are used to compute fold changes (FC). For
778 each pair of test/control samples, obtained FCs for all genes are ranked in increasing order.
779 Resulting ranks are associated to genes. Then, the k ranks of each gene are used to calculate a
780 statistic and resulting probability (f-value) used to identify the DEGs after fixing the error level
781 at 5% False Discovery Rate (FDR).

782 We performed the functional differential analysis using GAGE (93) and grouped all the
783 pathways into 8 functional categories (noted meta-pathways). The functional intermodel meta-
784 pathway connectivity was studied identifying the genes shared between pathways and models
785 inside the same meta-pathway. Then, to assess the gene connectivity we build a minimum fully
786 connected protein-protein interaction (PPI) network (noted MinPPINet) of genes known to be
787 involved in synaptic function as they were associated with synaptic pathways via GO (94) and
788 KEGG databases (95) and furthermore added regulatory information to build the final
789 RegPPINet. We used the betweenness centrality analysis to identify hubs, keys for maintaining
790 the network communication flow. The relevance of the connecting nodes was further predicted
791 by the machine learning algorithm Quack (96). Finally, we computed 100000 random networks
792 with a similar degree, to assess if the likelihood of observing such connectivity in the DS
793 network was more than one can expect by chance using statnet and sna R packages
794 (https://cran.r-project.org/web/packages/statnet/index.html; https://cran.r-
795 project.org/web/packages/sna/index.html).

796

797 **Visual stimulation**

798 Mice raised in a standard light cycle were housed in constant darkness for two weeks.
799 Then, animals in the light-exposed condition group, were consecutively exposed to light for 0,
800 1, 3, or 7.5 h before being sacrificed. Instead, animals part of the dark-housed condition group

were sacrificed in the dark. After euthanasia, their eyes were enucleated before the visual cortex dissection in the light and flash frozen in liquid nitrogen. cDNA and quantitative PCR were performed as indicated in the supplementary information. The Ct values were transformed to quantities by using the comparative Ct method. Hence, all data were expressed relative to the expression of the most expressed gene. This relative expression levels, were normalized with Genorm by keeping the more stable reference genes (97). To calculate fold-induction, relative quantity of gene expression at each time point was divided by the mean of relative level of gene expression of dark housed mice for corresponding genotype. The mean and standard error were calculated at each time point from these fold-induction values.

Statistical analysis

All data are expressed as mean group value ± standard error of the mean (SEM) or as box plots with the median and quartiles . For each data set, we analysed if the data was normally distributed by Shapiro–Wilk test and Quantile-Quantile plots (Supplementary fig 2) and the homogeneity of variances by the Brown-Forsy test. Differences between groups were inferred by one-way ANOVA (Open field) and ANOVA for repeated measures, or in case of datasets where the assumptions of normality or homogeneity of variances were not fulfilled we performed the Kruskal-Wallis non-parametric test. The post hoc tests (Fisher LSD Method) were conducted only if the F parameter in ANOVA achieved 0.05 level. All the behavioral analysis results are found in Supplementary table 1. For MRI data, intergroup comparisons on region-based data were conducted on the normalized volumes (i.e., ratio between the volume of the structure and the whole brain volume) of each segmented structure using the Student t-test while correcting by multiple testing setting up a FDR correction.

Acknowledgements

We would like to thank members of the research group, of the IGBMC laboratory and of the ICS. We are grateful to the IGBMC microarray and Sequencing platform and particularly C. Thibault-Carpentier, for providing us access to microarray. We extend our thanks to the animal care-takers of the ICS who are in charge of the mice wellness. We also thank F.Riet, C. Mittelhaeuser, A. Lux and V. Alunni and D. Dembele for expert technical assistance and useful discussion.We would like to aknowledge that Maria del Mar Muñiz Moreno was an IGBMC International PhD Programme fellow supported by LabEx INRT funds (ANR-10-LABX-0030-INRT).

Competing interests

The authors have no competing interest. This work has been supported by the National Centre for Scientific Research (CNRS), the French National Institute of Health and Medical Research (INSERM), the University of Strasbourg (Unistra), the French state funds through the “Agence Nationale de la Recherche” under the frame programme Investissements d’Avenir labelled ANR-10-IDEX-0002-02, ANR-10-LABX-0030-INRT, ANR-10-INBS-07 PHENOMIN to YH. The funders had no role in study design, data collection and analysis, decision to publish, or preparation of the manuscript.

References

1. Lejeune J, Turpin R, Gautier M. [Mongolism; a chromosomal disease (trisomy).]. Bull Acad Natl Med. 1959;143(11-12):256-65.
2. Antonarakis SE, Lyle R, Dermitzakis ET, Reymond A, Deutsch S. Chromosome 21 and down syndrome: from genomics to pathophysiology. Nat Rev Genet. 2004;5(10):725-38.
3. Oliver TR, Feingold E, Yu K, Cheung V, Tinker S, Yadav-Shah M, et al. New insights into human nondisjunction of chromosome 21 in oocytes. PLoS Genet. 2008;4(3):e1000033.
4. McCormick MK, Schinzel A, Petersen MB, Stetten G, Driscoll DJ, Cantu ES, et al. Molecular genetic appoach to the characterization of the "Down syndrome region" of chromosome 21. Genomics. 1989;5(2):325-31.
5. Korbel JO, Tirosh-Wagner T, Urban AE, Chen XN, Kasowski M, Dai L, et al. The genetic architecture of Down syndrome phenotypes revealed by high-resolution analysis of human segmental trisomies. Proceedings of the National Academy of Sciences of the United States of America. 2009;106(29):12031-6.
6. Korenberg JR. Molecular mapping of the Down syndrome phenotype. Prog Clin Biol Res. 1990;360:105-15.
7. Lyle R, Béna F, Gagos S, Gehrig C, Lopez G, Schinzel A, et al. Genotype-phenotype correlations in Down syndrome identified by array CGH in 30 cases of partial trisomy and partial monosomy chromosome 21. Eur J Hum Genet. 2009;17(4):454-66.
8. Delabar JM, Theophile D, Rahmani Z, Chettouh Z, Blouin JL, Prieur M, et al. Molecular mapping of twenty-four features of Down syndrome on chromosome 21. Eur J Hum Genet. 1993;1(2):114-24.
9. Korenberg JR, Chen XN, Schipper R, Sun Z, Gonsky R, Gerwehr S, et al. Down syndrome phenotypes: the consequences of chromosomal imbalance. Proc Natl Acad Sci U S A. 1994;91(11):4997-5001.
10. Rahmani Z, Blouin JL, Creau-Goldberg N, Watkins PC, Mattei JF, Poissonnier M, et al. Critical role of the D21S55 region on chromosome 21 in the pathogenesis of Down syndrome. Proc Natl Acad Sci U S A. 1989;86(15):5958-62.
11. Herault Y, Delabar JM, Fisher EMC, Tybulewicz VLJ, Yu E, Brault V. Rodent models in Down syndrome research: impact and future opportunities. Disease Models & Mechanisms. 2017;10(10):1165-86.
12. Gupta M, Dhanasekaran AR, Gardiner KJ. Mouse models of Down syndrome: gene content and consequences. Mammalian Genome. 2016;27(11-12):538-55.
13. Muñiz Moreno MDM, Brault V, Birling MC, Pavlovic G, Herault Y. Modeling Down syndrome in animals from the early stage to the 4.0 models and next. Prog Brain Res. 2020;251:91-143.
14. Herault Y, Duchon A, Velot E, Marechal D, Brault V, Dierssen M, et al. The in vivo Down syndrome genomic library in mouse. Down Syndrome: From Understanding the Neurobiology To Therapy. 2012;197:169-97.
15. Reeves RH, Irving NG, Moran TH, Wohn A, Kitt C, Sisodia SS, et al. A MOUSE MODEL FOR DOWN-SYNDROME EXHIBITS LEARNING AND BEHAVIOR DEFICITS. Nature Genetics. 1995;11(2):177-84.
16. Duchon A, Raveau M, Chevalier C, Nalesso V, Sharp AJ, Herault Y. Identification of the translocation breakpoints in the Ts65Dn and Ts1Cje mouse lines: relevance for modeling down syndrome. Mammalian Genome. 2011;22(11-12):674-84.
17. Reinholdt LG, Ding YM, Gilbert GT, Czechanski A, Solzak JP, Roper RJ, et al. Molecular characterization of the translocation breakpoints in the Down syndrome mouse model Ts65Dn. Mammalian Genome. 2011;22(11-12):685-91.

18. Davisson MT, Schmidt C, Reeves RH, Irving NG, Akeson EC, Harris BS, et al. Segmental trisomy as a mouse model for Down syndrome. Prog Clin Biol Res. 1993;384:117-33.
19. Li Z, Yu T, Morishima M, Pao A, LaDuca J, Conroy J, et al. Duplication of the entire 22.9 Mb human chromosome 21 syntenic region on mouse chromosome 16 causes cardiovascular and gastrointestinal abnormalities. Hum Mol Genet. 2007;16(11):1359-66.
20. Olson LE, Richtsmeier JT, Leszl J, Reeves RH. A chromosome 21 critical region does not cause specific Down syndrome phenotypes. Science. 2004;306(5696):687-90.
21. Olson LE, Roper RJ, Baxter LL, Carlson EJ, Epstein CJ, Reeves RH. Down syndrome mouse models Ts65Dn, Ts1Cje, and Ms1Cje/Ts65Dn exhibit variable severity of cerebellar phenotypes. Dev Dyn. 2004;230(3):581-9.
22. Olson LE, Roper RJ, Sengstaken CL, Peterson EA, Aquino V, Galdzicki Z, et al. Trisomy for the Down syndrome 'critical region' is necessary but not sufficient for brain phenotypes of trisomic mice. Hum Mol Genet. 2007;16(7):774-82.
23. Belichenko NP, Belichenko PV, Kleschevnikov AM, Salehi A, Reeves RH, Mobley WC. The "Down syndrome critical region" is sufficient in the mouse model to confer behavioral, neurophysiological, and synaptic phenotypes characteristic of Down syndrome. J Neurosci. 2009;29(18):5938-48.
24. Pennington BF, Moon J, Edgin J, Stedron J, Nadel L. The neuropsychology of Down syndrome: evidence for hippocampal dysfunction. Child Dev. 2003;74(1):75-93.
25. Nadel L. Down's syndrome: a genetic disorder in biobehavioral perspective. Genes Brain Behav. 2003;2(3):156-66.
26. Brown SDM, Hancock JM, Gates H. Understanding mammalian genetic systems: The challenge of phenotyping in the mouse. Plos Genetics. 2006;2(8):1131-7.
27. Mandillo M, Tucci V, Holter SM, Meziane H, Al Banchaabouchi M, Kallnik M, et al. Reliability, robustness, and reproducibility in mouse behavioral phenotyping: a cross-laboratory study. (vol 34, pg 243, 2008). Physiological Genomics. 2010;40(3):217-.
28. Ishihara K, Amano K, Takaki E, Shimohata A, Sago H, Epstein CJ, et al. Enlarged Brain Ventricles and Impaired Neurogenesis in the Ts1Cje and Ts2Cje Mouse Models of Down Syndrome. Cerebral Cortex. 2010;20(5):1131-43.
29. Raveau M, Nakahari T, Asada S, Ishihara K, Amano K, Shimohata A, et al. Brain ventriculomegaly in Down syndrome mice is caused by Pcp4 dose-dependent cilia dysfunction. Human Molecular Genetics. 2017;26(5):923-31.
30. Guedj F, Pereira PL, Najas S, Barallobre MJ, Chabert C, Souchet B, et al. DYRK1A: A master regulatory protein controlling brain growth. Neurobiology of Disease. 2012;46(1):190-203.
31. Guedj F, Sebrie C, Rivals I, Ledru A, Paly E, Bizot JC, et al. Green Tea Polyphenols Rescue of Brain Defects Induced by Overexpression of DYRK1A. Plos One. 2009;4(2):8.
32. Gardiner K, Fortna A, Bechtel L, Davisson MT. Mouse models of Down syndrome: how useful can they be? Comparison of the gene content of human chromosome 21 with orthologous mouse genomic regions. Gene. 2003;318:137-47.
33. Brault V, Duchon A, Romestaing C, Sahun I, Pothion S, Karout M, et al. Opposite phenotypes of muscle strength and locomotor function in mouse models of partial trisomy and monosomy 21 for the proximal Hspa13-App region. PLoS Genet. 2015;11(3):e1005062.
34. Duchon A, Herault Y. DYRK1A, a Dosage-Sensitive Gene Involved in Neurodevelopmental Disorders, Is a Target for Drug Development in Down Syndrome. Frontiers in Behavioral Neuroscience. 2016;10.
35. Nguyen TL, Duchon A, Manousopoulou A, Loaëc N, Villiers B, Pani G, et al. Correction of cognitive deficits in mouse models of Down syndrome by a pharmacological inhibitor of DYRK1A. Dis Model Mech. 2018;11(9).

36. Faizi M, Bader PL, Tun C, Encarnacion A, Kleschevnikov A, Belichenko P, et al. Comprehensive behavioral phenotyping of Ts65Dn mouse model of Down Syndrome: Activation of pradrenergic receptor by xamoterol as a potential cognitive enhancer. Neurobiology of Disease. 2011;43(2):397-413.
37. Souchet B, Guedj F, Sahun I, Duchon A, Daubigney F, Badel A, et al. Excitation/inhibition balance and learning are modified by Dyrk1a gene dosage. Neurobiology of Disease. 2014;69:65-75.
38. Escorihuela RM, Fernández-Teruel A, Vallina IF, Baamonde C, Lumbreras MA, Dierssen M, et al. A behavioral assessment of Ts65Dn mice: a putative Down syndrome model. Neurosci Lett. 1995;199(2):143-6.
39. Martinez-Cue C, Baamonde C, Lumbreras M, Paz J, Davisson MT, Schmidt C, et al. Differential effects of environmental enrichment on behavior and learning of male and female Ts65Dn mice, a model for Down syndrome. Behavioural Brain Research. 2002;134(1-2):185-200.
40. Martinez-Cue C, Rueda N, Garcia E, Davisson MT, Schmidt C, Florez J. Behavioral, cognitive and biochemical responses to different environmental conditions in male Ts65Dn mice, a model of Down syndrome. Behavioural Brain Research. 2005;163(2):174-85.
41. Moran TH, Capone GT, Knipp S, Davisson MT, Reeves RH, Gearhart JD. The effects of piracetam on cognitive performance in a mouse model of Down's syndrome. Physiol Behav. 2002;77(2-3):403-9.
42. Rueda N, Florez J, Martinez-Cue C. Effects of chronic administration of SGS-111 during adulthood and during the pre- and post-natal periods on the cognitive deficits of Ts65Dn mice, a model of Down syndrome. Behavioural Brain Research. 2008;188(2):355-67.
43. Rueda N, Florez J, Martinez-Cue C. Chronic pentylenetetrazole but not donepezil treatment rescues spatial cognition in Ts65Dn mice, a model for Down syndrome. Neuroscience Letters. 2008;433(1):22-7.
44. Seo H, Isacson O. Abnormal APP, cholinergic and cognitive function in Ts65Dn Down's model mice. Exp Neurol. 2005;193(2):469-80.
45. Lockstone HE, Harris LW, Swatton JE, Wayland MT, Holland AJ, Bahn S. Gene expression profiling in the adult Down syndrome brain. Genomics. 2007;90(6):647-60.
46. Prandini P, Deutsch S, Lyle R, Gagnebin M, Vivier CD, Delorenzi M, et al. Natural gene-expression variation in Down syndrome modulates the outcome of gene-dosage imbalance. American Journal of Human Genetics. 2007;81(2):252-63.
47. Ait Yahya-Graison E, Aubert J, Dauphinot L, Rivals I, Prieur M, Golfier G, et al. Classification of human chromosome 21 gene-expression variations in Down syndrome: impact on disease phenotypes. American journal of human genetics. 2007;81(3):475-91.
48. Laffaire J, Rivals I, Dauphinot L, Pasteau F, Wehrle R, Larrat B, et al. Gene expression signature of cerebellar hypoplasia in a mouse model of Down syndrome during postnatal development. Bmc Genomics. 2009;10.
49. Sultan M, Piccini I, Balzereit D, Herwig R, Saran NG, Lehrach H, et al. Gene expression variation in 'Down syndrome' mice allows to prioritize candidate genes. Genome Biol. 2007;8(5):R91.
50. Mao R, Zielke CL, Zielke HR, Pevsner J. Global up-regulation of chromosome 21 gene expression in the developing Down syndrome brain. Genomics. 2003;81(5):457-67.
51. Olmos-Serrano JL, Kang HJ, Tyler WA, Silbereis JC, Cheng F, Zhu Y, et al. Down Syndrome Developmental Brain Transcriptome Reveals Defective Oligodendrocyte Differentiation and Myelination. Neuron. 2016;89(6):1208-22.
52. Guedj F, Pennings JL, Massingham LJ, Wick HC, Siegel AE, Tantravahi U, et al. An Integrated Human/Murine Transcriptome and Pathway Approach To Identify Prenatal Treatments For Down Syndrome. Sci Rep. 2016;6:32353.

53. Guedj F, Pennings JL, Wick HC, Bianchi DW. Analysis of adult cerebral cortex and hippocampus transcriptomes reveals unique molecular changes in the Ts1Cje mouse model of down syndrome. Brain Pathol. 2015;25(1):11-23.
54. Aziz NM, Guedj F, Pennings JLA, Olmos-Serrano JL, Siegel A, Haydar TF, et al. Lifespan analysis of brain development, gene expression and behavioral phenotypes in the Ts1Cje, Ts65Dn and Dp(16)1/Yey mouse models of Down syndrome. Dis Model Mech. 2018;11(6).
55. Joazeiro CAP. Mechanisms and functions of ribosome-associated protein quality control. Nature Reviews Molecular Cell Biology. 2019;20(6):368-83.
56. Woods YL, Cohen P, Becker W, Jakes R, Goedert M, Wang X, et al. The kinase DYRK phosphorylates protein-synthesis initiation factor eIF2Bepsilon at Ser539 and the microtubule-associated protein tau at Thr212: potential role for DYRK as a glycogen synthase kinase 3-priming kinase. Biochem J. 2001;355(Pt 3):609-15.
57. Hong SH, Lee KS, Kwak SJ, Kim AK, Bai H, Jung MS, et al. Minibrain/Dyrk1a regulates food intake through the Sir2-FOXO-sNPF/NPY pathway in Drosophila and mammals. PLoS Genet. 2012;8(8):e1002857.
58. Hernández-González S, Ballestín R, López-Hidalgo R, Gilabert-Juan J, Blasco-Ibáñez JM, Crespo C, et al. Altered distribution of hippocampal interneurons in the murine Down Syndrome model Ts65Dn. Neurochem Res. 2015;40(1):151-64.
59. Shukkur EA, Shimohata A, Akagi T, Yu WX, Yamaguchi M, Murayama M, et al. Mitochondrial dysfunction and tau hyperphosphorylation in Ts1Cje, a mouse model for Down syndrome. Human Molecular Genetics. 2006;15(18):2752-62.
60. King MK, Pardo M, Cheng YY, Downey K, Jope RS, Beurel E. Glycogen synthase kinase-3 inhibitors: Rescuers of cognitive impairments. Pharmacology & Therapeutics. 2014;141(1):1-12.
61. Mardinly AR, Spiegel I, Patrizi A, Centofante E, Bazinet JE, Tzeng CP, et al. Sensory experience regulates cortical inhibition by inducing IGF1 in VIP neurons. Nature. 2016;531(7594):371-5.
62. Spiegel I, Mardinly AR, Gabel HW, Bazinet JE, Couch CH, Tzeng CP, et al. Npas4 Regulates Excitatory-Inhibitory Balance within Neural Circuits through Cell-Type-Specific Gene Programs. Cell. 2014;157(5):1216-29.
63. Smith GK, Kesner RP, Korenberg JR. Dentate Gyrus Mediates Cognitive Function in the Ts65Dn/DnJ Mouse Model of Down Syndrome. Hippocampus. 2014;24(3):354-62.
64. Belichenko PV, Kleschevnikov AM, Becker A, Wagner GE, Lysenko LV, Yu YE, et al. Down Syndrome Cognitive Phenotypes Modeled in Mice Trisomic for All HSA 21 Homologues. 2015(1932-6203 (Electronic)).
65. Yu T, Liu CH, Belichenko P, Clapcote SJ, Li SM, Pao AN, et al. Effects of individual segmental trisomies of human chromosome 21 syntenic regions on hippocampal long-term potentiation and cognitive behaviors in mice. Brain Research. 2010;1366:162-71.
66. Chakrabarti L, Best TK, Cramer NP, Carney RSE, Isaac JTR, Galdzicki Z, et al. Olig1 and Olig2 triplication causes developmental brain defects in Down syndrome. Nature Neuroscience. 2010;13(8):927-U39.
67. Xu R, Brawner AT, Li S, Liu JJ, Kim H, Xue H, et al. OLIG2 Drives Abnormal Neurodevelopmental Phenotypes in Human iPSC-Based Organoid and Chimeric Mouse Models of Down Syndrome. Cell Stem Cell. 2019;24(6):908-26 e8.
68. Ermak G, Cheadle C, Becker KG, Harris CD, Davies KJA. DSCR1 (Adapt78) modulates expression of SOD1. Faseb Journal. 2004;18(1):62-9.
69. Voronov SV, Frere SG, Giovedi S, Pollina EA, Borel C, Zhang H, et al. Synaptojanin 1-linked phosphoinositide dyshomeostasis and cognitive deficits in mouse models of Down's syndrome. Proceedings of the National Academy of Sciences of the United States of America. 2008;105(27):9415-20.

70. Antonarakis SE. Down syndrome and the complexity of genome dosage imbalance. Nat Rev Genet. 2016.
71. Chen C-K, Bregere C, Paluch J, Lu JF, Dickman DK, Chang KT. Activity-dependent facilitation of Synaptojanin and synaptic vesicle recycling by the Minibrain kinase. Nature Communications. 2014;5.
72. De la Torre R, De Sola S, Pons M, Duchon A, Martinez de Lagran M, Farre M, et al. Epigallocatechin-3-gallate, a DYRK1A inhibitor, rescues cognitive deficits in Down syndrome mouse models and in humans. Molecular Nutrition & Food Research. 2014;58(2):278-88.
73. Altafaj X, Martin ED, Ortiz-Abalia J, Valderrama A, Lao-Peregrin C, Dierssen M, et al. Normalization of Dyrk1A expression by AAV2/1-shDyrk1A attenuates hippocampal-dependent defects in the Ts65Dn mouse model of Down syndrome. Neurobiology of Disease. 2013;52:117-27.
74. Garcia-Cerro S, Martinez P, Vidal V, Corrales A, Florez J, Vidal R, et al. Overexpression of Dyrk1A Is Implicated in Several Cognitive, Electrophysiological and Neuromorphological Alterations Found in a Mouse Model of Down Syndrome. Plos One. 2014;9(9).
75. Dunnett SB, Everitt BJ, Robbins TW. THE BASAL FOREBRAIN CORTICAL CHOLINERGIC SYSTEM - INTERPRETING THE FUNCTIONAL CONSEQUENCES OF EXCITOTOXIC LESIONS. Trends in Neurosciences. 1991;14(11):494-501.
76. Isacson O, Seo H, Lin L, Albeck D, Granholm AC. Alzheimer's disease and Down's syndrome: roles of APP, trophic factors and ACh. Trends in Neurosciences. 2002;25(2):79-84.
77. Hamlett ED, Boger HA, Ledreux A, Kelley CM, Mufson EJ, Falangola MF, et al. Cognitive Impairment, Neuroimaging, and Alzheimer Neuropathology in Mouse Models of Down Syndrome. Current Alzheimer Research. 2015;13(1):35-52.
78. Salehi A, Delcroix JD, Belichenko PV, Zhan K, Wu CB, Valletta JS, et al. Increased App expression in a mouse model of Down's syndrome disrupts NGF transport and causes cholinergic neuron degeneration. Neuron. 2006;51(1):29-42.
79. Lee HC, Tan KL, Cheah PS, Ling KH. Potential Role of JAK-STAT Signaling Pathway in the Neurogenic-to-Gliogenic Shift in Down Syndrome Brain. Neural Plast. 2016;2016:7434191.
80. Ling KH, Hewitt CA, Tan KL, Cheah PS, Vidyadaran S, Lai MI, et al. Functional transcriptome analysis of the postnatal brain of the Ts1Cje mouse model for Down syndrome reveals global disruption of interferon-related molecular networks. BMC Genomics. 2014;15:624.
81. de la Torre R, de Sola S, Hernandez G, Farre M, Pujol J, Rodriguez J, et al. Safety and efficacy of cognitive training plus epigallocatechin-3-gallate in young adults with Down's syndrome (TESDAD): a double-blind, randomised, placebo-controlled, phase 2 trial. Lancet Neurology. 2016;15(8):801-10.
82. Nakano-Kobayashi A, Awaya T, Kii I, Sumida Y, Okuno Y, Yoshida S, et al. Prenatal neurogenesis induction therapy normalizes brain structure and function in Down syndrome mice. Proc Natl Acad Sci U S A. 2017;114(38):10268-73.
83. Herault Y, Delabar JM, Fisher EMC, Tybulewicz VLJ, Yu E, Brault V. Rodent models in Down syndrome research: impact and future opportunities. Dis Model Mech. 2017;10(10):1165-86.
84. Marechal D, Brault V, Leon A, Martin D, Pereira PL, Loaëc N, et al. Cbs overdosage is necessary and sufficient to induce cognitive phenotypes in mouse models of Down syndrome and interacts genetically with Dyrk1a. Hum Mol Genet. 2019.
85. Marechal D, Lopes Pereira P, Duchon A, Herault Y. Dosage of the Abcg1-U2af1 region modifies locomotor and cognitive deficits observed in the Tc1 mouse model of Down syndrome. PLoS One. 2015;10(2):e0115302.

86. Guedj F, Pereira PL, Najas S, Barallobre MJ, Chabert C, Souchet B, et al. DYRK1A: a master regulatory protein controlling brain growth. Neurobiol Dis. 2012;46(1):190-203.
87. Hoelter SM, Dalke C, Kallnik M, Becker L, Horsch M, Schrewe A, et al. "Sighted C3H" mice - a tool for analysing the influence of vision on mouse behaviour? Frontiers in Bioscience. 2008;13:5810-23.
88. Dubos A, Meziane H, Iacono G, Curie A, Riet F, Martin C, et al. A new mouse model of ARX dup24 recapitulates the patients' behavioural and fine motor alterations. Hum Mol Genet. 2018.
89. Arbogast T, Iacono G, Chevalier C, Afinowi NO, Houbaert X, van Eede MC, et al. Mouse models of 17q21.31 microdeletion and microduplication syndromes highlight the importance of Kansl1 for cognition. PLoS Genet. 2017;13(7):e1006886.
90. Ung DC, Iacono G, Méziane H, Blanchard E, Papon MA, Selten M, et al. Ptchd1 deficiency induces excitatory synaptic and cognitive dysfunctions in mouse. Mol Psychiatry. 2017.
91. Arbogast T, Ouagazzal AM, Chevalier C, Kopanitsa M, Afinowi N, Migliavacca E, et al. Reciprocal Effects on Neurocognitive and Metabolic Phenotypes in Mouse Models of 16p11.2 Deletion and Duplication Syndromes. PLoS Genet. 2016;12(2):e1005709.
92. Dembele D, Kastner P. Fold change rank ordering statistics: a new method for detecting differentially expressed genes. Bmc Bioinformatics. 2014;15.
93. Luo W, Friedman MS, Shedden K, Hankenson KD, Woolf PJ. GAGE: generally applicable gene set enrichment for pathway analysis. BMC Bioinformatics. 2009;10:161.
94. Ashburner M, Ball CA, Blake JA, Botstein D, Butler H, Cherry JM, et al. Gene ontology: tool for the unification of biology. The Gene Ontology Consortium. Nat Genet. 2000;25(1):25-9.
95. Esling P, Lejzerowicz F, Pawlowski J. Accurate multiplexing and filtering for high-throughput amplicon-sequencing. Nucleic Acids Res. 2015;43(5):2513-24.
96. Desai AP, Razeghin M, Meruvia-Pastor O, Pena-Castillo L. GeNET: a web application to explore and share Gene Co-expression Network Analysis data. PeerJ. 2017;5:e3678.
97. Vandesompele J, De Preter K, Pattyn F, Poppe B, Van Roy N, De Paepe A, et al. Accurate normalization of real-time quantitative RT-PCR data by geometric averaging of multiple internal control genes. Genome Biology. 2002;3(7).

Supporting information

S1 Fig. Down syndrome mouse models analysed in the study. In the upper part of the plot the human chromosome 21 is represented, in yellow we highlighted the Hsa21 syntenic region found in mouse from *Lipi* to *Zbtb21* (known as *Zfp295* previously). The eight models analysed on this study Dp1Yey, Dp3Yah, Ts65Dn, Dp5/Dp1, Dp5Yah, Dp1Rhr, Tg(*Dyrk1a*), Dp5yah crossed with Tg(*Dyrk1a*) (noted as Dp5-Tg)) trisomic chomosomal regions were draw in comparison with the Hsa21 region.

S2 Fig. Quantile-Quantile plots to assess Normal distribution. The quantile-quantile plots (Q-Q plots) and Shapiro-Wilk test for the following behavioural datasets: Y-maze, NOR and OF were analysed to study how well our data could be modelled following a normal distribution. Only the distance travelled in OF did not reach the statistical significance level in the Shapiro-Wilk test.

S3 Figure. DS mouse models and Morris water maze. The MWM results are presented as distance travelled to reach the platform (A), speed (B) and % of distance travelled in the peripheral zone (C, Mean ± SEM). Ts65Dn mice were drastically impaired with an increase in distance travelled to reach the platform and in the distance travelled along the peripheral zone. Less drastically Tg(*Dyrk1a*) mice showed an increased distance travelled to escape the pool and in the peripheral zone (* $p<0.05$, ** $p<0.01$, *** $p<0.001$).

S4 Fig. DS mouse models and context and cue fear conditioning. The fear conditioning results are presented as inactivity periods in seconds (Mean±SEM). Only Ts56Dn mice present an impairment in context fear conditioning (* $p<0.05$, ** $p<0.01$, *** $p<0.001$).

S5 Fig. Comparison of the Z-score calculated from the MRI volume of different brain structures from the DS models. The structures affected in Tg(*Dyrk1a*) were also affected in Dp1Yey and Ts65Dn, whereas the Dp1Rhr mice.(Dp1Yey n=6wt and 6 Tg ; Ts65Dn n=5 wt and 6 Tg ; Tg(*Dyrk1a*) n=8 wt and 5 Tg ; Dp1Rhr n=7 wt and 7 Tg).

S6 Fig. Fold change expression levels of the genes analysed by the microarrays homologous to the Hsa21 mouse chromosome 16 (mm16). The genes are displayed following the order of their genomic start site coordinates. The duplicated areas for each mouse model appear shaded in the following colours, purple, grey, aquamarine, red, blue and golden for Dp1Yey, Dp3Yah, Ts65Dn, Dp1Rhr, Dp5Yah and Tg(*Dyrk1a*) respectively.

S7 Fig. Fold change expression levels of genes analyzed by the microarrays. (A) Fold change expression levels of the genes analysed by the microarrays part of the centromeric region of the mouse chromosome 17. The centromeric region of the mouse chromosome 17, is defined by the UCSC table browser as the region between the coordinates chr17:110000-3000000.The genes are displayed following the order of their start site genomic coordinates. The region duplicated in the Ts65Dn model non homologous to the hsa21, appears shaded in aquamarine. (B) Fold change expression levels of the genes homologous to the Hsa21 in mouse

chromosome 10 (mm10) and chromosome 17 (mm17) analysed by the microarrays. The genes are displayed following the order of their start site genomic coordinates.

S8 Fig. Number of deregulated probes per chromosomes per models. Trisomic mice have similar patterns with a pic of deregulated genes located on mouse chromosome 16. Tg Dyrk1a at contrary, present a global pattern of deregulated probes.

S9 Fig. Overview of the top 7 dysregulated genes (higher significance and fold change difference) for each mouse model over the global transformed expression profiles illustrated over volcano plots. The x axis and y axis represent the log2 fold change of the genes expression and the log transformed FDR values respectively. The genes whose fcros FDR value <0.05 are considered significant. These genes are represented in purple or pink and labelled as "Significant". Instead the genes whose abs (FC)> 1.4 are represented in green or pink and labelled "FC". Finally, the genes that don't comply these conditions are considered not significant.

S10 Fig. Gene expression correlation analyses. (A) Correlation of the 4328 differentially expressed genes (DEGs) expression levels on the different models. B) Correlation of the 75 differentially expressed trisomic genes (TEGs) expression levels on the different models. Each row represents a model pairwise correlation with the rest of the models. The density and histograms distribution of the gene expression values for each model is found in the medial diagonal (Black for DEGs, and pink for TEGs). The LOESS smoothed fit is represented by a red line. The plots were created in R using the pairs.panel function from Psych R CRAN package (28).

S11 Fig. Weighted networks representing the connectivity of the pathways included in the Cell structure & organelles, and the Transcription & epigenomic regulation meta-pathways. (A) Representation of the strength connecting the pathways included on the Cell Structure & organelle meta-pathway. (B) Representation of the strength connecting the pathways included on the Transcription & epigenomics regulation meta-pathway. The pathways incorporated in each meta-pathway were identified in the differential functional analysis (DFA) by GAGE after imposing a q-val <0.1 cut off. The connectivity between the pathways, (the edges weight or strength connecting the pathways) is represented by the number of altered genes identified by GAGE shared by each two pathways and is calculated based on the number of common genes within the pathways shared inter and intra mouse model (by each mouse model multi group defined) also grouped by regulation sense using the following formula* and represented by the thickness of the edges connecting the nodes (pathways) of the network. Each edges colour depends on the mouse models where those genes were identified (mouse model multi groups). Formula* = number of genes shared by each pathway on each model on each sense of regulation * factorRes with factorRes= 0.6.

S12 Fig. Weighted networks representing the connectivity of the pathways included in the Ribosome and Mitochondrial meta-pathways. (A) Representation of the strength connecting the pathways included on the Ribosome meta-pathway. (B) Representation of the strength connecting the pathways included on the Mitochondria meta-pathway. The pathways incorporated in each meta-pathway were identified in the differential functional analysis (DFA) by GAGE after imposing a q-val <0.1 cut off. The connectivity between the pathways, (the

edges weight or strength connecting the pathways) is represented by the number of altered genes identified by GAGE shared by each two pathways and is calculated based on the number of common genes within the pathways shared inter and intra mouse model (by each mouse model multi group defined) also grouped by regulation sense using the following formula* and represented by the thickness of the edges connecting the nodes (pathways) of the network. Each edges colour depends on the mouse models where those genes were identified (mouse model multi groups). Formula* = number of genes shared by each pathway on each model on each sense of regulation * factorRes with factorRes= 0.6

S13 Fig. Weighted network representing the connectivity of the pathways included in the Synaptic meta-group and the network representation of the genes linked to Interferon Beta (IFN-B) ungrouped pathway. (A) Representation of the strength connecting the pathways included on the Synaptic meta-pathway. The pathways incorporated in each meta-pathway were identified in the differential functional analysis (DFA) by GAGE after imposing a q-val <0.1 cut off. The connectivity between the pathways, (the edges weight or strength connecting the pathways) is represented by the number of altered genes identified by GAGE shared by each two pathways and is calculated based on the number of common genes within the pathways shared inter and intra mouse model (by each mouse model multi group defined) also grouped by regulation sense using the following formula* and represented by the thickness of the edges connecting the nodes (pathways) of the network. Each edges colour depends on the mouse models where those genes were identified (mouse model multi groups). Formula* = number of genes shared by each pathway on each model on each sense of regulation * factorRes, factorRes= 0.6. (B) Genes linked to Interferon Beta (IFN-B) ungrouped pathway, found altered in the different mouse model multi groups by GAGE. The genes are represented by the ellipse shapes instead the mouse model multi groups by lilac cuadrangles. If the genes were found up regulated then a red boder color was used around the ellipses. The genes also identified by FCROS as differentially expressed (DEG) were identified by a red colored inner ellipse.

S14 Fig. Protein-protein interaction and regulatory gene connectivity networks (RegPPINets) of genes involved in the synaptic meta-pathway highlighting biological cascades connectivity. The two sub-networks (A and B) were extracted from the STRING04 MinPPINet. This network was built querying STRING and selecting the PPIs with a medium confidence score (CS), CS=0.4 from all sources of evidence, and was further annotated with regulatory information using REACTOME (See Supplementary material and Methods). The shapes of the nodes represent the following information: Shapes: i)Pallid pink ellipses: represent connecting proteins added to assure the full connectivity of the network; ii) pink octagons, represent HSA21 syntenic genes in mouse not identified as contributing to the meta-pathway dysregulation by GAGE; iii) green inner coloured ellipses, genes identified by GAGE after q-val <0.1 cut off to be contributing even slightly, to any pathway of those found dysregulated inside the meta-pathway. If the size is similar to the octagons, they are also HSA21 syntenic genes in mouse. Additionally, the border colour represents the mouse model multi group where those genes are found altered in; iv) diamonds, genes identified by GAGE after q-val <0.1 cut off and also by FCROS as DEGs. (A) RegPPINet Sub-network extracted from the selection of RHOA 2^{nd} interactors from STRING04 MinPPINet, highlighting RHOA 1^{st} Interactors and DYRK1A and GSK3B interactors annotated with the regulatory information from REACTOME. (B) RegPPINet Sub-network extracted from the selection of NPAS4 2^{nd} interactors from STRING04 MinPPINet. Inside of the ellipsoidal line shapes we highlighted NPAS4 interactors involved in the regulation of GABA receptors (cyan), of NMDA receptors (orange), SNARE complex (purple), RHOA (pink), GSK3B (Blue), both RHOA and GSK3B (black) and the genes linked to mitochondrial, ribosomal and cytoskeleton activity (yellow).

S15 Fig. Expression level of genes of interest in the different DS models. Different panels to show the expression level of genes of interest located or not in the region homologous to Hsa21. Data are presented as boxplot plots of th ratio of trisomic on disomic with the median and quartiles (Stastitical analysis was done comparing wt and mutant value with a student t test, * $p<0.05$, ** $p<0.01$, *** $p<0.001$).

S16 Fig. Detection of RHOA and the phoshorylated form of Myosin Light Chain (P-MLC) by Western blot in Dp1Yey hippocampal lysates and their control (wt) littermates. (A) Western blot of RHOA showed no changes in RHOA protein levels in the Dp1Yey line compared to their wt littermates (wt (n=5) and Dp1Yey (n=5)). (B) Western blot of P-MLC revealed a statistically significant decrease (* $p < 0.05$) in the amount of this protein in Dp1Yey mice (wt (n=5) and Dp1Yey (n=5)) (Student's t-test: wt vs. Dp1Yey $t(8) = 2,392$; $p = 0,0437$).

S1 Table: Summary of behavioural results including statistical assessment.

S2 Table. Volumes of each brain structure (in mm3) normalized by total brain volume derived from MRI region-based analysis.

S3 Table. Summary of the DEA and DFA results for each trisomic DS model. We included the number of trisomic genes with compensated or partially compensated expression levels, approximately half of the trisomic genes are compensated and the overall identity of DEGs are different between the models.

S4 Table. Fold-change of the gene expression in trisomic (Tg) compared to the controls for each mouse model dataset. The genes included on thoses lists were used to produce the supplementary figs 6 and 7 as follows: i) genes included inside the duplicated genomic regions of chr 16, ii) genes included inside the Ts65Dn chr17 duplicated region iii) genes of the centromeric region of chr17.

S5 Table. Pathways identified by GAGE as dysregulated including the genes contributing to each altered pathway per each mouse model multi group combination and including the name of the meta-pathway assignated.